Accepted Manuscript

Lateral and vertical variations in sedimentology and geochemistry of sub-horizontal laminated travertines (Çakmak quarry, Denizli Basin, Turkey)

Zahra Mohammadi, Hannes Claes, Enrico Capezzuoli, Mahtab Mozafari, Jeroen Soete, Cihan Aratman, Rudy Swennen

PII: S1040-6182(18)30730-4

DOI: https://doi.org/10.1016/j.quaint.2018.11.041

Reference: JQI 7661

To appear in: *Quaternary International*

Received Date: 27 May 2018

Revised Date: 12 October 2018

Accepted Date: 30 November 2018

Please cite this article as: Mohammadi, Z., Claes, H., Capezzuoli, E., Mozafari, M., Soete, J., Aratman, C., Swennen, R., Lateral and vertical variations in sedimentology and geochemistry of sub-horizontal laminated travertines (Çakmak quarry, Denizli Basin, Turkey), *Quaternary International* (2019), doi: https://doi.org/10.1016/j.quaint.2018.11.041.

Lateral and vertical variations in sedimentology and geochemistry of sub-horizontal laminated travertines (Çakmak quarry, Denizli Basin, Turkey)

Zahra, Mohammadi.[1], Hannes, Claes.[1], Enrico Capezzuoli.[2], Mahtab Mozafari.[3], Jeroen Soete.[1], Cihan Aratman.[1,4], and Rudy Swennen.[1]

[1]Department of Earth and Environmental Sciences, KU Leuven, Celestijnenlaan 200E, Leuven B-3001, Belgium

[2]Department of Physics and Geology, University of Perugia, Italy

[3]Department of Chemistry, Life Sciences and Environmental Sustainability, University of Parma, Italy

[4]Department of Geological Engineering, Pamukkale University, Denizli, Turkey

*email: zahra.mohammadi@kuleuven.be

Mail to: rudy.swennen@kuleuven.be

Abstract

The laterally extensive sub-horizontal laminated travertine deposits outcropping in the Çakmak quarry (Denizli Basin, Turkey) allows reconstructing their three-dimensional geobody architecture. Based on field observations, detailed petrographic and geochemical analyses (stable carbon and oxygen isotopes, major and trace elements) the most important controlling porosity-permeability parameters in this lacustrine-dominated facies, in relation to microfacies and diagenetic modifications were constrained. Sedimentological analyses and the observed architectural geometries allowed to subdivide the sub-horizontal carbonate succession into three main depositional units. These units in turn, based on macro- and microscopic observations were subdivided into nine dominant lithotypes reflecting an overall shrub flat and a marsh pool depositional setting. The shrub flat facies mainly comprises dendritic shrub crusts boundstone, pustular grainstone and clotted micrite mudstone to boundstone. In contrast, the marsh pool environment is dominated by coated reed rudstone to boundstone, cryptalgal silty bioclast-rich bioturbated mudstone and peloidal packstones.

The diagenetic study revealed that the sediments were affected by dissolution, cementation, sparmicritization, recrystallization, and local formation of Fe-oxi/hydroxides and chalcedony. Among the diagenetic products, in particular, the calcite cements were investigated, applying micro-analysis of stable carbon and oxygen isotopes. Accordingly, the co-variation between the obtained isotopic values and the elemental concentrations (Sr, Mg, Na, and S) point to a thermogene fluid system that likely circulated through the subsurface limestones, dolomites and evaporites of the Lycian Nappes. These findings ensure an in-depth understanding of continental carbonate deposition, i.e. sub-aqueous travertines, in the context of a lacustrine depositional system.

Keywords: shrub-like fabrics, sub-horizontal facies, stable isotope, sedimentology and diagenesis

1. Introduction

Since Roman times travertine carbonates have mainly been used as a building material. By the end of the ’90, the scientific interest for this rock type increased in relation with its applications in various research fields including tectonics (Altunel and Hancock, 1993a, 1993b, 1996; Altunel, 1994; Hancock et al., 1999; Mesci et al., 2008; Brogi and Capezzuoli, 2009, 2014), palaeoclimate (Yan et al., 2012; Wang et al., 2014), facies analysis (Guo and Riding, 1998; Pentecost, 2005; Capezzuoli et al., 2014; Ronchi and Cruciani, 2015; Della Porta, 2015; Claes et al., 2015, 2016; Erthal et al., 2017), stable isotope geochemistry (Andrews et al., 1993; Fouke et al., 2000; Andrews and Riding, 2001; Kele et al., 2008, 2011; Fouke, 2011), geobody architecture (Claes et al., 2015, 2016), petrophysical analysis (Soete et al., 2015, 2017) and reservoir characteristics (Soete et al., 2015; Ronchi and Cruciani, 2015; Claes et al., 2015, 2017; De Boever et al., 2016; Schröder et al., 2016). The latter interest is related to the relatively recent hydrocarbon reservoir discoveries offshore South America and offshore West Africa in continental carbonate deposits (the so-called Pre-salt deposits) (Carminatti et al., 2008). The study of travertine outcrops as potential reservoir analogues is considered as an effective alternative to study the reservoir properties and controlling parameters (e.g. lithotype and diagenesis) in these heterogeneous carbonates. The latter relates to the high variability in architecture, lithotypes, diagenesis and petrophysical properties. Of key importance within the Pre-salt setting are shrub-like fabrics that developed within a lacustrine setting (Dias, 1998, 2005; Carminatti et al., 2008; Wright, 2012; Rezende and Pope, 2015; Saller et al., 2016) and that also have been reported from lacustrine travertine environments (e.g. Erthal et al., 2017). The current study focuses on a sub-aqueous depositional system of extended sub-horizontal laminated travertines in the Çakmak quarry (Turkey). Sub-horizontal laminated travertine deposits outcrop in the lower part of the Çakmak, Faber, Ece, Alimoğlu, Ilik quarries, and extend over at least 2 by 1.5 km^2 (Van Noten et al., 2013; Claes et al. 2015, 2017), of which a part has been characterised in detail in this study. Despite the fact that the travertines from the Ballik area have been studied by Özkul et al. (2002, 2013), Claes et al. (2015) and De Boever et al. (2016), no detailed information is yet available about the sub-horizontal travertines, that according to these authors developed in a lacustrine-like setting. Claes et al. (2017) worked out a widely applicable classification for shrub-like fabrics and their pore typology. The lateral continuity and the transition from one shrub-type to another, in function of the palaeoenvironmental setting, have been addressed by Erthal et al. (2017) in the case of the Tivoli travertines (central Italy). These variations are not only of importance for the reconstruction of the depositional environment but are also of interest from a hydrocarbon reservoir point of view since they potentially instigate reservoir variability. Consequently, in this study, the vertical as well as lateral lithotype variations inside the sub-horizontal travertines and their depositional setting are addressed. In addition, the thermogene nature of these travertines based on stable carbon and oxygen isotope signatures (Pentecost, 2005; Gandin and Capezzuoli, 2008; Kele et al., 2008, 2011; Teboul et al., 2016) is highlighted. A microscopic sampling of cement and micrite phases was executed in order to compare the sedimentological from the diagenetic signature. Early diagenetic cements negatively affected porosity and permeability, however, they also reinforce the rock framework, resulting in a higher mechanical strength that would hamper porosity-permeability decrease during compaction (e.g. Soete et al., 2015). Therefore, it is essential to determine the diagenetic overprints, such as precipitation of cements. Furthermore, chemical analyses were carried out in order to address some of the geochemical signatures pointing to their origin. Finally, since microbial activity is often linked to the development of shrub fabrics in sub-horizontal travertines (Krumbein et al., 1977; Chafetz and Folk, 1984; Chafetz, 1986; Buczynski and Chafetz, 1991; Guo and Riding, 1992; Vasconcelos and McKenzie, 1997; Dupraz et al., 2004, 2009; Vasconcelos et al., 2013; Chafetz, 2013, Erthal et al., 2017), TOC analyses were carried out to deduce possible microbial interferences, also considering organic carbon isotope signature and C/N ratios.

This study thus (i) considers small-scale lithotype variations providing a systematic framework related to the palaeo-environmental evolution in a sub-aqueous system; (ii) focuses on the micro-analysis of carbon and oxygen stable isotopes to study the nature and spatial distribution of cements and matrix in continental carbonates and (iii) ultimately provides a conceptual model for the evolution of the sedimentary palaeoenvironment in this sub-horizontal laminated travertine succession. Consequently, this study improves our understanding of the processes that affect the reservoir architecture within sub-aqueous travertines.

2. Geological setting

The study area is situated in the Denizli Basin, which is Early Burdigalian in age (Alçiçek, 2010). This graben of approximately 50 by 24 km is located in the Western Anatolian Extensional Province of Turkey (Fig. 1). This basin is bound by normal faults along its northern and southern margins (Koçyiğit, 2005; Westaway et al., 2005; Alçiçek et al., 2007, 2013). The Denizli Basin is the continuation of the E–W-trending Büyük Menderes Graben, the NW–SE-trending Gediz Graben and the Küçük Menderes Graben (Özkul et al., 2002, 2013; Kele et al., 2011; Van Noten et al., 2013). In the Denizli area, the rollback subduction of the North African oceanic crust below the Anatolian plate led to uplift, associated with exhumation and subsequent relaxation, with an extensional collapse, resulting in a horst-graben structure (Westaway, 1993; Westaway et al., 2005; van Hinsbergen et al., 2010; Gürbüz et al., 2012). The central part of the Denizli Basin comprises two Quaternary sub-basins, namely the Laodikeia Graben in the south and the Çürüksu Graben in the north (Koçyiğit, 2005). The latter, which is a Neogene-Quaternary depression, is of interest in this study. Pre-Neogene bedrock, consisting of the Palaeozoic-Mesozoic Menderes Massif, Triassic carbonates and evaporites and the Upper Cretaceous thrusted Lycian Nappes, is exposed at the northern and southern margins of the Denizli Basin. The Menderes Massif is composed of metamorphosed rock units (Alçiçek et al., 2007). The Lycian Nappes are subdivided into the Lycian Thrust Sheets, the Lycian Mélange and the Lycian Ophiolites (Sözbilir, 2005). The lithologies forming the Lycian Nappes are dolomitic limestones, marbles, sandstones, ophiolitic mélanges and evaporites (Alçiçek et al., 2007).

The Ballık study area is located in the southeastern part of Denizli Basin at the intersection of the Çürüksu and Baklan Grabens (Van Noten et al., 2013). Where continental carbonates are exposed along its northern flank, it is subdivided into a northernmost so-called "upper area", containing more than 10 travertine quarries, and a lower "domal area". The latter contains several large travertine quarries (e.g. Best Abandoned, Alimoğlu, Çakmak, İllik, Faber and Ece quarries) in which the lowermost excavated part consists of sub-horizontal laminated travertines (Van Noten et al., 2013). The WNW-ESE oriented Çakmak quarry (37^0 51'44.71" N, 29^0 20' 35.66" E) forms one of the largest excavations in the southern flank of the "domal area". Previous researchers (Claes et al., 2015; De Boever et al. 2016) have described the "domal area" as consisting of five different lithofacies, from old to young, sub-horizontal facies/extended pond, non-carbonate marls/conglomerates, smooth-sloping cascade, steep-sloping waterfall and reed facies (Figs. 2 and 3). The development of these continental carbonates and non-carbonates took place through several evolutionary steps (Fig. 3A). Their precipitation commenced with formation of the sub-horizontal strata in a shallow sub-aqueous environment (Fig. 3A sequences 1). The substrate upon which these deposits formed consisted of unlithified siliciclastic sediments (Curewitz and Carson, 1999). This system evolved into non-carbonate marls/conglomerates, likely related to a change in climatic conditions (Verbiest et al., 2018) (Fig. 3A sequences 2, 4 and 5) followed by renewed dome shape travertine deposition of smooth-sloping cascade, steep-sloping waterfall and reed facies (De Boever et al., 2016) (Fig. 3A sequences 3). This study focuses on the sub-horizontal strata which are located within the lower 15 m of the vertical quarry wall, and are exposed over an area of about 400 by 350 m. The studied sub-horizontal facies were one of the lithofacies reported by De Boever et al. (2016). However, a detailed study of this facies, as presented in this paper, has not been reported before. This study focuses on the sub-horizontal strata and report for the first time on the internal organisation of the rock fabrics and existing variations of these sub-horizontal deposits (Figs. 2 and 3).

3. Methodology

3.1 Field observations, petrography and mineralogy

The lateral and vertical sedimentological characteristics along the lower part of the quarry walls were described, photographed, and logged to address µm to m-scale variations. 120 horizontal representative core plugs were collected along 14 logs performed on the quarry walls. Samples were impregnated with blue resin, and thin sections were prepared. Some samples were also impregnated with fluorescent resin to highlight (micro)-porosity. Lithotype and diagenetic features were studied in thin sections by traditional light, fluorescence (Leica DM LP equipped with a fluorescence lamp 12/100 W, type: 301e391.010 with BP450-490/LP515 filter set) and cathodoluminescence (CL) microscopy (modified Technosyn 9200MK2 operated at 15 kV and 300–400 µA gun current). CL colours will only be mentioned where luminescence was encountered. Most of the samples are, however, non-luminescent. In addition, a scanning electron microscope (SEM, model Hitachi TM-1000) with magnifications up to 11000x was used to study the micro-fabrics of fresh-cut, un-polished surfaces. The mineralogy of 12 samples was determined by X-ray powder diffraction (XRD) using a Philips PW 1930 diffractometer.

3.2 Stable carbon and oxygen isotopes

In order to enhance the accuracy of isotope measurements and to clearly distinguish the values obtained for cement and micrite, a micromill device with a drill bit of 100 μm diameter was used to collect sample powders with microdrill-holes of 25 μm deep. 71 powders were collected in 12 ml Labco Exetainers. Samples were analysed on a Thermo Delta V Advantage isotope ratio mass spectrometer coupled to a GasBench II. In the laboratory, samples were flushed with helium and reacted with 100% phosphoric acid to produce CO_2 gas. Samples were allowed to react for 24 hours at 25°C to reach isotopic equilibrium. Data from each run were corrected using the regression method with LSVEC ($\delta^{18}O$ = −26.7‰, $\delta^{13}C$ = −46.6‰), NBS-19 ($\delta^{18}O$ = −5.01‰, $\delta^{13}C$ = −23.2‰), and NBS-19 ($\delta^{18}O$ = −2.2‰, $\delta^{13}C$ = +1.95‰) as standards, as well as using two in-house $CaCO_3$ standards, which were regularly calibrated against NBS-19 and LSVEC. Long-term standard deviations were better than 0.1‰. Both $\delta^{18}O$ and $\delta^{13}C$ values of samples are expressed relative to VPDB (Vienna Pee Dee Belemnite).

3.3 Major and trace element geochemistry (ICP-OES)

Inductively Coupled Plasma - Optical Emission Spectroscopy (ICP-OES) was used to analyse the concentration of major and trace elements in 114 samples. The elemental composition of travertines allows linkage to fluid composition and eventually to the source rock and the hydrological system (Teboul et al., 2016). Samples were selected to represent different stages in the evolution of the travertine body and to detect variations between different lithotypes. Before analysis, the samples were dissolved according to a four acids digestion protocol , which allows for the dissolution of carbonates and non-carbonate constituents that possibly could result from detrital influx or diagenetic processes. For analysis, 100 mg of powdered sample was weighed and put into Teflon beakers. The four acids used for digestion of the samples were HNO_3 (14M or 65%, sub-boiled), $HClO_4$ (70%, pro analysis Sigma Aldrich), HF (49%, sub-boiled) and HCl

(2.5M). The digestion of the samples in the acids was done on two hotplates. First 3 ml HNO_3 was added, turning the temperature to 200°C, allowing to evaporate during 40 minutes. Subsequently, 3 ml of $HClO_4$ was added and "cooked" for 1 hour at 230°C. Once a large drop was left (about 0.5 ml), 3 ml HF was added at 240°C and digested until almost dry. Finally, 7 ml HCl was added and heated for 15 minutes. All samples were fullydissolved, i.e. no residue remained, so no filtering was required. In the final step, the sample solution was diluted up to 25 ml with MilliQ water. To determine the detection limit and the analytical accuracy, two reference samples and two blanks (one per hot-plate) included in the study.

3.4 TOC

15 mg of representative lithotype travertine samples were weighed into 9x5 mm Ag cups, and carbonates were removed by repeated acidification with diluted (2%) HCl. For the determination of %OC (organic carbon), %N (nitrogen) and the stable carbon isotope composition of the OC fraction ($\delta^{13}C_{OC}$), samples were combusted in an elemental analyser – isotope ratio mass spectrometer (EA-IRMS, ThermoFinnigan Flash HT, and ThermoFinnigan DeltaV Advantage), and data were calibrated using an in-house Leucine and IAEA-C600 standard (caffeine).

4. Field observations

Within the sub-horizontal facies, on the basis of the continuous lateral correlation markers, which reflect breaks in the travertine precipitation (i.e. exposure surfaces), and lithotype association, three different units were distinguished (Fig. 4). These units that can be laterally followed over several hundreds of meters, exhibit sedimentary structures with slightly different orientations.

Unit 1 (2-4 m thick) displays a low dipping angle (< 10°) to the E-SE. The top is marked by an erosional surface that laterally can be followed as a non-travertine deposits . It is composed of compact white with a faint brownish hue horizontal bed, which contrasts with the typical white coloured travertines.

Unit 2 (4-9 m thick) displays a gradual steepening from sub-horizontal phyto-boundstones above the lower non-travertine deposits evolving into very low angle (< 5°) micro-terrace deposits. The boundary between Unit 2 and 3 consists of alternating flat to wavy laminae. The latter are cut off the deposits by a red-stained exposure surface (Figs. 4E and F).

Unit 3 (4 m thick) consists of a smooth slope facies and a low angle terrace slope facies, which are locally bordered by steeper laminae defining the pool rims. The smooth slope facies laterally changes to flat sub-horizontal facies. Towards the northwestern side of the quarry, these strata change into flat laminae. .

5. Petrography and lithotype description

Nine travertine lithotypes and a marker horizon of non-travertine deposits were differentiated based on meso- to micro-scale characteristics and stratal architecture within the sub-horizontal travertine facies (Fig. 5), from which five lithotypes (i.e. L4, 5, 6, 7 and 9) have been previously reported by researchers addressed in Table 1. This study therefore will mostly focus on providing additional observations on the aforementioned lithotypes, and introducing new detailed lithotypes based on recent findings. First the lithotypes will be described, which is then followed by a brief interpretation. Lithotype is here defined as the macro-scale appearance of the microscopic fabric organization (see Claes et al., 2015). Fabric analysis relied on reported studies from other localities by Folk and Chafetz (1983), Guo and Riding (1999), Sant'Anna et al. (2004), Jones and Renaut (2010), Barilaro et al. (2012), Gandin and Capezzuoli (2014), Della Porta (2015) and Croci et al. (2016), as well as from the studied Ballik area (Turkey) by Claes et al. (2017) and Tivoli area (Italy) by Erthal et al. (2017). The rock type terminology used in this study is based on Dunham (1962) and Embry and Klovan (1971). The classification of shrubs is based on morphology reported by Chafetz and Guidry (1999), Claes et al. (2017) and Erthal et al. (2017).

Dendritic shrub boundstone

At macro-scale dendritic shrub boundstone makes up undulating layers of bright white to creamy travertine, with regular geometric shrub morphologies with arborescent and arbustiform outline. This lithotype can be followed laterally and vertically over more than 100 m and 7 m, respectively. The thickness of the individual layers that contain dendritic shrub crusts changes from 5 mm to 2 cm (Figs. 6A, B, C). They are bordered at their bottom and top by millimeter sized peloidal grainstone. At microscopic scale, dendritic shrub boundstone consists of bush-like structures, with dendritic outlines consisting of fibrous (Figs. 7A, B) as well as wide dendritic structures (Figs. 7C, D) diverging from a central nucleation centre (root-like structure) (Fig. 7E). The latter are sometimes surrounded by thin calcite cement rims up to 1-2 mm in length and 2- 5 mm in width. The dendritic fabrics occur adjacent to each other, as dense and tightly packed clotted structures. The primary voids is reduced by spar crystals. Intershrub, intrashrub and interdigit growth framework porosity, interlaminar porosity, microporosity and mouldic porosity are the characteristic pore types in this lithotype, which appear in most cases partially reduced by cement (Fig. 7D).

Interpretation

This lithotype displays micritic aggregates of regular morphology making up dendritic shrubs well described in literature (Guo and Riding, 1992, 1999; Folk and Chafetz, 1983; Chafetz and Folk, 1984; Chafetz and Guidry, 1999; Chafetz, 2013). Some characteristics such as regular morphology, micrite aggregation and microporosity represent some similarity with microbially mediated shrubs described by the above-mentioned authors. More specifically, presence of fauna or flora (e.g. ostracods, rarely cyanobacteria-like structures and microbial filaments) in some cases can be attributed to appropriate environmental conditions where microbial activity likely was prolific. However, no distinct evidence regarding the presence of microbes was found. Based on the observed microbial textures (Riding, 2000), the lack of distinct fluorescence microscopical observation, and low TOC values, support the dominance of abiotic travertine precipitation. Therefore, abiotic processes likely dominantly influenced the development of Çakmak shrub structures. The shrubs are laterally persistent in wavy crust structures making up almost straight to slightly inclined layers, pointing to deposition in gently sloping micro-terraced settings. Some lateral variations, from proximal to distal environment (with regard to spring), have been noticed where the branch morphology of dendritic shrubs changes from narrow and elongated to wider and shorter widespread shrub morphotypes often with interdigitated pore shapes (Figs. 7A to F). Thus, shrub morphology seems to be influenced by hydrodynamic conditions (as stated by Erthal et al. 2017) as well as by pre-existent small-scale topography. Incomplete growth structures usually occur in laterally restricted laminae in distal parts, suggesting shrub growth under low energy conditions. This may likely be related to occur at times of sudden saturation increase as a consequence of evaporation in stagnant water within distal locations , i.e. away from the spring areas. Here the micritic aggregation resulted in broadleaf, wide-branching shrub structures. The shrub accumulations are – as a rule - laterally and vertically continuous over several meters. They often change into clotted micritic mudstone to boundstone, which can result from a decrease in water-flow energy or a change in topography.

Pustular shrub grainstone: on macro-scale, the pustular shrub grainstones are characterised by white, tightly cemented, sub-rounded shrubs varying from 0.1 to 4 mm in size (Fig. 6F). Lateral continuity of this lithotype is commonly extensive in layers of centimeters to maximum one meter in thickness. It occurs laterally, but discontinuously, over the entire study area. The pustular grains are relatively homogeneous in size and morphology. On microscopic scale they show densely packed micritic clumps with uniform internal structure (Fig. 7G). The limited size of the pustular shrubs points to their stunted growth origin, compared to dendritic shrubs. This lithotype is associated with dendritic shrubs. While there is a complete absence of microporosity in the pustular shrub structures, grainstones display a large intershrub growth framework porosity, which is partially filled with cement.

Interpretation

Based on Dias (1998), the pustular shrubs result from undeveloped branches of arborescent shrubs as a consequence of local physico-chemical and biological conditions. Chafetz and Guidry (1999) suggested that pustular shrubs originate from broken “leaves” of bacterial shrubs that formed under periodic turbulence. In our case they show good sorting, but the roundness of the individual pustules is not perfect, which can relate to the reworking but over a restricted transport distance. Hence, the formation of pustular shrubs probably took place after decrease in turbulence in a water column where they accumulated and made up lenticular bodies at the bottom and behind the obstacles. Their patchy accumulation in small depressions between other lithotypes supports this hypothesis (Fig. 6E). This lithotype is laterally extensive, however discontinued locally, within lacustrine marshy environments and distal parts of shrub flats. Vertically and laterally they are usually interfingering or occur adjacent to dendritic shrubs and spongy boundstones as well as coated eroded reed fragments.

Radial shrub packstone/grainstone: on macro-scale the radial shrub packstones/grainstones display spherical and rounded to sub-spherical to sub-rounded white coloured grains, 1 to 5 mm in size (Fig. 6G). They contain cores that are in some cases partially dissolved. This lithotype occurs widespread in the study area, especially in the areas most far away from the assumed springs. They form horizontal lenses of 10 to 60 cm in thickness and up to 40 cm of vertical extent. Microscopically this lithotype reveals an irregular to regular concentric radial shrub morphology that develops around a nucleus, which appears alongside clotted peloids floating in a microsparitic matrix (Fig. 7H and I). Intershrub growth framework porosity, microporosity and interdigit growth framework porosity can be observed within this lithotype, which in some cases are partially to entirely reduced by cement (e.g. equant calcite cement).

Interpretation

This lithotype resembles to some extent the pisoid travertine described by Guo and Riding (1999) and the radial pisoids of Chafetz and Folk (1984). Similar lithologies have been described by Rainey and Jones (2009), Della Porta (2015) and Croci et al. (2016). According to several of these authors, pools on terraced slopes and flat depressions are suitable places for their formation. Their rounded shape with internal radial branches point towards small shallow ponds for their formation. An organic influence on the generation of the internal radially structured shape is supported by the abundance of bacterial-like coccoid structures, as also reported by Chafetz and Guidry (1999). In addition, the varying amount of microporosity is likely the result of bacterial decay. The size of the microporosity (3-4 µm in size), observed in several samples, is in accordance with such microbial activity. Radial shrubs display some similarity in their lateral extension comparable to pustular shrubs. Vertically, they usually occur between lower-energy lithotypes such as mudstone and clotted micrite and lithotypes reflecting higher-energy environments like shrub crusts. This lithotype usually develops in the bottom part of shrub flats and lacustrine settings. They vertically and laterally usually interfinger or are associated by dendritic shrubs and spongy boundstones and even coated eroded reeds.

Clotted micrite packstone to boundstone: at the macro-scale, this lithology consists of compact gray-coloured travertines with layers that range from centimetres to metres in thickness. This lithotype usually alternates vertically with silty mudstone and peloidal packstone. Microscopically these strata are made up of dense micrite referred to as “micrite islands” (*sensu* Riding, 2000). Clotted micrites are usually surrounded by bladed calcite cement of 50 - 100 µm in length (Fig. 9F), which in some cases show mottled orange luminescence patterns. The most important porosity type observed is microporosity, fracture, vuggy and micro-biomouldic pores. The latter especially derive from dissolution of cyanobacteria, algae, gastropod and ostracod shells and are filled by equant calcite cement.

Interpretation

Clotted micrite can be interpreted as microbially mediated precipitation with evidence of cyanobacteria, coccolith bacteria and algae. In most cases some biofilms of cyanobacteria, filaments and diatoms can be observed, but intense decomposition prevents identification of the exact species. In addition, according to Dupraz et al. (2004), Extracellular Polymeric Substances (EPS) can also mediate precipitation of similar structures. In the latter case it acts as a place for carbonate nucleation and when after precipitation the EPS is destroyed, it leaves behind only traces. As already stated by many authors (e.g. Monty, 1976; Freytet and Plet, 1996; Gierlowski-Kordesch, 2010; Croci et al., 2016), micrite is deposited around and within microbial communities like cyanobacteria especially in stationary water pool settings. According to Golubić et al. (2009), without EPS, precipitation of calcium carbonate would still occur, but it would be much slower. These mudstones to boundstones can be made up of homogeneous micrite, which points to an authigenic origin of the micrite clumps. Turbulent waters finally may tear up, rework and transport the initial micrite as individual grains. The latter case implies transportation of travertine intraclasts, which can be interpreted as resulting from upstream, lithified and eroded travertine (Guo and Riding, 1999; Rainey and Jones, 2009; Gandin and Capezzuoli, 2014). They have rather large lateral extent and vertically they are often related to mudstone in lacustrine parts of marsh environments. Finally, they often exhibit some luminescence that likely relates to recrystallization.

Non-travertine deposits:

Non-travertine deposit form a thin horizon containing reworked material (e.g. siliciclastic and clay) that has been transported formed by local pedogenesis. It can be easily recognized as a horizon due to the presence of palaeokarst features associated with it and the dark grey colour in outcrop. Its thickness varies from 15 cm to 20 cm and can be followed laterally over a distance of more than 100 m (see Fig. 4B). In the upper part consists of angular breccia fragments of travertine within a brown clay matrix. The tips of associated reed moulds are inclined towards the NW.

Interpretation

The encountered horizon are the products of travertine alteration under influence of rainwater, biological activity and evaporation during periods of exposure. This exposure is due to a decrease or cessation of fluid discharge from the vent(s) (e.g. Guo and Riding, 1999; Flügel, 2010). Variations in vent location and/or direction of water flow may also result in widespread exposure (Chafetz and Folk, 1984; Guo and Riding, 1999; Faccenna et al., 2009; Özkul et al., 2002, 2014). Local travertine fragments inside this horizon suggests that they may have been subject to erosion especially during the last stage of development of this horizon. They likely reflect a pedogenic overprint combined with layers testifying to deposition of erosional material from the hinterland, thus corresponding to kinds of sheet-floods taking place during periods of emergence. These fragments displaying imbricated-like structures indicate up-current orientation patterns and high water-flow energy, which may reflect fluvial activity or some sheet flooding from SE direction. Moreover, presence of plant relicts at the top of this horizon reflects subsequent suitable conditions for plant growth, indicating palustrine conditions. Their inclination is towards the NW.

6. Diagenetic features and porosity types

The major diagenetic processes affecting the sub-horizontal travertines of the Çakmak quarry are cementation, dissolution, spar-micritization, recrystallization, and formation of authigenic minerals. XRD analyses indicated that on average 96% of the studied travertine is composed of calcite. The other 4% consists of quartz, Fe-oxi/hydroxide, manganese oxide, and clay minerals, as can also be inferred from the geochemical analysis.

Carbonate dissolution and organic decay resulted in vug to cavity development (Figs. 10C to F) and (enlarged) reed mouldic porosity (Fig. 10F). Their size can reach up to 10 cm in diameter and exceptionally 80 cm in length. Larger cavities may be partially filled by rafts (Fig. 10D) and small stalagmite-like structures while cavity walls are sometimes covered by coarse banded calcite cement (see Fig. 10C). Moreover, solution enlarged fractures of 1 to 4 m in length were observed. These features thus testify of intra-depositional dissolution, whereby cavities in the past were sometimes partially or completely water filled. Apart from the dissolution cavities creating porosity, a wide range of micron to centimetre sized pores occur, being depositional in origin or relating to the decay of organic material. Depositional porosity includes shrub- and phyto-framework porosity, observed in dendritic shrub and reed lithotypes and intergranular porosity particularly observed within the pustular shrubs, radial shrubs (see Figs. 7H and I) and coated grains. Fluorescence microscopy reveals low microporosity in the dendritic shrub crust boundstone, while the clotted and peloidal textures show well-connected microporosity. Secondary porosity is mostly observed in the form of bio-mouldic reed-, ostracod- and gastropod-mouldic porosity. Fenestral-like porosity is present in both peloidal and spongy-microbial travertines (see Fig. 9A and B). Vuggy porosity originates from solution enlargement of other pore types. It occurs in all lithotypes. Vuggy pores can be connected (see Fig. 9G) or isolated (see Fig. 9I). Finally, intra-crystalline porosity occurs between cement crystals (see Fig. 9I). The lowest porosity was observed in mudstone lithotypes while the highest porosity occurs in the spongy lithotype.

The cements are generally non-luminescent calcites. They include: (1) Fibrous, bladed cements and dogtooth cement rims (Figs. 11A, B and C); (2) Blocky and equant mosaic cement (Figs. 11D and E) usually filling intergranular, vuggy and mouldic pores; (3) Isopachous banded crystal - micrite couplets in which micro-lamination inside the cements reflects different cement growth stages (Figs. 11A, F and G) and (4) Meniscus-cement at or near coated grain contacts (Fig. 11H).

Recrystallization is evidenced by orange to dull luminescence and undulose extinction involving several adjacent crystals. Clotted micrite inclusions in spar crystals also evidence recrystallization. These phenomena are mostly observed in clotted micrite and dendritic shrub fabrics (Figs. 12B, C). SEM analyses show theoccurrence of spar-micritization in both clotted micrite and mudstones. Finally, formation of authigenic minerals, including trace amounts of chalcedony and dendritic oxides/hydroxides, were observed in mudstones.

7. Geochemistry

7.1 Stable carbon and oxygen isotopes

To avoid mixing of different fabrics and cements micro-sampling for stable isotope analysis was applied. The values of analysed components are shown in Appendix 1. The $\delta^{13}C$ values of all analysed carbonates vary between –0.4 and +3.7‰. The $\delta^{18}O$ values of micrite and cement phases range between –9.4 and –5.7‰. The $\delta^{13}C$ signature for the individual units plots in discrete but overlapping clusters. Unit 1, 2 and 3 have $\delta^{13}C$ values varying from +0.9 to +3.7‰, +0.2 to +2.1‰ and –0.4 to +1.7‰, respectively. The $\delta^{18}O$ values obtained for these units range between –7.9 to –5.9‰, –7.6 to –5.7‰ and –9.4 to –6.7‰, respectively (Figs. 13 and 14). In Unit 1 and 2 $\delta^{13}C$ values from micrite are often more enriched than in the cements, while in Unit 3 they vary around a similar mean value. Micrite shows relatively depleted $\delta^{18}O$ signatures in comparison to the cements in Unit 1 (with the exception of one sample) while micrite becomes more often less depleted in comparison to the cements within Unit 2. In Unit 3 no clear trend can be deduced (Figs. 15 and 16).

7.2 Major and trace element geochemistry

The elemental concentrations of major elements (Ca and Mg) and trace elements (Al, Fe, Mn, K, Ti, P, Ba, Sr, Ni, As and Rb) are given in Appendix 2. The concentrations do not show any specific trend in function of the different lithotypes. However, the co-variation among the concentrations of Al, Fe and K is obvious in the vicinity of the non-travertine deposits. These concentrations generally appear as outliers (>1000 µg/g) among the recorded values. The high concentration of these elements with respect to the normal ranges known for travertine (Pentecost, 2005) relates to the presence of non-carbonate components, in particular, clay minerals. The Fe and Mn concentrations, excluding the above-mentioned samples, are within the expected range reported by Pentecost (2005). Moreover Sr, Mg, S and Na concentrations clearly display some co-variation. The non-travertine deposits is not considered.

7.3 TOC

Measured Total Organic Carbon (TOC), stable carbon and nitrogen isotopic compositions and C/N ratio obtained from the different TOC samples demonstrate variations within and between lithotypes (Table 2). The OC values show an average of 0.17 % with highest value of 0.25% in the reed lithotype and lowest value of 0.09% in the fully cemented radial shrub lithotype. The C/N ratios range between 2.27 to 4.62 (mean 3.90). The lowest value is measured within the fully cemented radial shrub. The highest ratios occur in the reed lithotype. The $\delta^{13}C_{OC}$ values vary from -14.5 to -24.6‰ (mean -22.0‰) in radial shrubs and mudstones, respectively. The $\delta^{15}N$ values range from -0.1 to +3.4‰ (mean + 1.4‰). Among the samples, the clotted micrite and reed samples show the lowest and highest values, respectively.

8. Discussion

8.1 Organic inferences

Total organic carbon (TOC), which is an indicator of organic matter content, has been analysed to infer whether additional arguments in favour of organic mediation of carbonate precipitation can be put forward. Moreover, it can provide indications on the type of depositional environment (e.g., lacustrine, fluvial, fissure ridge). The total organic matter content is, however, low, indicating a dominantly abiotic precipitation system rather than a biotic system. Despite these low values, the C/N ratio and carbon isotope signature can be used as indicators of the biota living in the settings where the aquatic sediments formed (Thornton and McManus, 1994; Meyers, 1997; Andrews et al., 1999). The carbon isotope values of TOC vary between -14.5 and

-24.5‰ and C/N ratio plots between 2.27 to 4.62 without a clear trend in function of type of samples. Comparison of the measured data with Bianchi (2007) points towards involvement of microalgae and microbes including bacteria, diatoms, green and blue-green microalgae. This result is in accordance with the petrographic observations, apart from the obvious presence of vascular plants, i.e. reeds. They should be characterised by high C/N ratios (100 to 1000). The low ratio, however, could be attributed to the colonization of bacterial populations (e.g., C/N ratios of 3 to 4; Rice and Hanson, 1984), covering vascular plants representing a dominant fraction of the total N thereby decreasing the bulk C/N ratio of this material. With regard to the organic carbon isotope signature, it is not possible to pinpoint the exact organic matter type within the different lithotypes. However, it likely reflects cyanobacteria based on the study by Hayes (2001). More specifically, the samples show values similar to lacustrine algae, which is in line with the inferred lacustrine depositional environment of the sub-horizontal travertines (Fig. 17).

8.2 Nature and source of parental fluids

Unit 1 is characterised by relatively more depleted $\delta^{13}C$ and more enriched $\delta^{18}O$ values in cements when compared to the micrite. As soil-derived carbon can lower the $\delta^{13}C$ signature and cooling normally increases the $\delta^{18}O$ values (Pentecost, 2005), one possible explanation for such a pattern in Unit 1 can be a larger contribution of infiltrating cold meteoric waters that passed locally through overlying soils situated uphill of the depositional setting affecting the precipitation of cements. This explanation is in agreement with the general trend in $\delta^{13}C$ values in both cement and micrite of Unit 1 indicating more depleted values towards the non-travertine deposits.

Unit 2 is characterised by relatively more depleted $\delta^{13}C$ and $\delta^{18}O$ values in cements when compared to the micrite. The possible explanation for such depletion both in $\delta^{13}C$ and $\delta^{18}O$ values could relate to differences in temperature and degassing. After the initial precipitation of micrite, because of the large water mass volume of within the lacustrine setting, the temperature of the fluids could have been slightly higher, lowering the reset $\delta^{18}O$ values. Furthermore, the intensity of degassing in such a water mass may slightly decline through time, and thus the fluids which previously precipitated micrite, may have precipitated cement in between the micritic components. The overall increase in water temperature and decrease in levels of degassing ensure a lighter isotopic signature of the cements. In such a case, the isotopic signature of cements that probably originated from dissolution and precipitation of pre-existing micrite would be masked due to the large water volume.

Unit 3 does not show clear systematic patterns in isotopic composition of the cement versus micrite, most likely resulting from mixing water discharge affected by evaporation and temperature fluctuations.

The $\delta^{13}C$ and $\delta^{18}O$ values obtained by micro-sampling (see Figs. 15 and 16) prove that the discrepancy between micrite and cement reflects a difference in fluid signature between the diagenetic and the primary fluids. However, one should be aware of the fact that the reasons for the variations in isotopic signature of micrite and cements, such as precipitation conditions in terms of the thermogenic water discharge, extra infiltration mixing of pre-existing water, seasonal variations, evaporation, temperature, and small-scale morphology variations of the depositional environment (deep, rough and steep) can be very complex.

A comparison between $\delta^{13}C$ and $\delta^{18}O$ values of all the three units shows a decreasing $\delta^{13}C$ trend from Unit 1 towards Unit 3, while the $\delta^{18}O$ values remain more or less similar. Generally, enriched $\delta^{13}C$ signature in travertine deposits has been attributed to CO_2 degassing (Fouke, 2000 and references therein) while not much effecting the $\delta^{18}O$ signature. Accordingly, the enriched $\delta^{13}C$ values in Unit 1 possibly reflect the highest accumulation and contribution of the fluids affected by prominent CO_2 degassing.

According to Pentecost (2005) travertines can be classified as thermogene (deep thermal processes) or as meteogene (meteoric), based on the origin of CO_2. Samples from the study area, both cement and micrite, show positive $\delta^{13}C$ values (with the exception of one outlier). The $\delta^{13}C$ and $\delta^{18}O$ values obtained by micro-sampling, plotted on the diagram of Teboul et al. (2016) in Figure 13, show a pattern that is in agreement with the isotopic signature of thermogene (hypogean) travertine as introduced by Pentecost (2005). Accordingly, the source rock likely consists of carbonates and/or igneous rocks (except carbonatites and ultramafics). Trace element analysis provides further constraints on the kind of fluid source(s) as well as on potential fluid/rock interactions. The obtained results indicate that the elemental concentrations do not show specific trends in function of facies and lithological units. This suggests precipitation under non-equilibrium condition. Based on the recorded co-variations between different elements as well as previous studies (Pentecost, 2005; Claes et al., 2015), the elements can be divided into two groups.

The first element group consists of Mg, S, Ba, Na and Sr and relates to intra basinal factors (i.e. the feeder discharge), and most importantly to the fluid composition. The co-variation of these elements possibly reflects the influence of fluids that interacted with evaporitic deposits, which would explain the high S and Na contents, with respective mean values of 1410 and 97.6 ppm. Moreover, according to Teboul et al. (2016), chemical elements participating in the formation of travertine deposits may originate from the alteration of source rocks, in association with either non-hydrothermal (epigean) or hydrothermal (hypogean) hydrogeological systems. Especially based on the Sr (ranging from 364 to 1599 ppm) and Ba (ranging from 4 to 327 ppm) cross plot, strong concentration differences in source rock and hydrologic regime can be inferred according to the latter authors (Fig. 18). With reference to the diagram of Teboul et al. (2016), the results of the studied samples plot in the field of limestones, evaporites and dolomites as source rock reflecting a thermogene system. Based on the lithostratigraphic section of the Denizli Basin, the most likely formation with the above-mentioned characteristics are the (Mesozoic) Lycian Nappes consisting of both limestone and evaporitic deposits. This interpretation is in full accordance with Claes et al. (2015) and El Desouky et al. (2015), who based their conclusion also on the Sr-isotope signatures recorded in the travertines. Notice also that other travertine deposits that have been studied in this Denizli Basin were also classified as thermogene (e.g. Pamukkale; Kele et al., 2011 and Alcicek et al., 2018).

The second element group, composed of Al, Fe, Mn, K, P and Ti, relates to the non-carbonate fraction reflecting external sediment input. This result is in agreement with petrographical observations, where clay and heavy minerals as well as detrital quartz and feldspar have been encountered. Group two displays elevated values especially in the non-travertine deposits, as well as in distal parts of the basin away from the springs.

Although, each of the studied units is characterised by a distinct stratigraphic pattern, the overlapping trend of the stable isotopic values suggests a similar source rock. Whether the small variations are related to changes in groundwater level and/or flow pathways cannot be deduced with certainty.

8.3 Local precipitation conditions and spring proximity

The synthesized geomorphological and sedimentological observations related to the depositional model are graphically represented in Fig. 19. By studying the Çakmak sub-horizontal layers as a representative outcrop of a flat depression, a more in depth understanding can be gained on its “building blocks”. Here the lateral variation evolves from smoothly sloping travertines as a part of micro-terraced travertines at the toe of the slope to a shrub flat environment, finally grading into a marsh environment, in line with the depositional model introduced by Guo and Riding (1998, 1999) for Rapolano Terme in Tuscany (central Italy). These deposits are gently prograding from Unit 1 to Unit 3, while the lateral and vertical distribution of the shrub flat and marsh environment is not uniform within them. The most continuous lithotype in the shrub flat environment corresponds to the dendritic shrub crust boundstone, and in the marsh environment to the peloidal packstone.

Despite the present-day south facing topography of the sub-horizontal strata, Van Noten et al. (2013) showed that the tectonic activity of the graben postdated the development of the sub-horizontal strata, explaining the existence of this facies in the uplifted northern flank with a different topography from the original depositional environment. This interpretation is in line with the pond development, since a pre-existed relief would have more likely resulted in formation of a cascade and/or waterfall facies rather than a sub-horizontal. The fact that the present-day topography of the sub-horizontal strata is not representative of the time of formation, the reconstruction of the paleoflow direction is based on the criteria such as different strata orientations, fossilized plant growth orientations, in particular reed, sedimentary structures (e.g. imbrications) and dip-orientation of the sedimentary features. Accordingly, the dominant paleoflow in Unit 1 were originally directed from the east-side of the quarry, and changed to northeast in Unit 2, and eventually to north in Unit 3 (see Fig. 5). The comparison with active analogues (e.g. Pamukkale) supports changing spring location and or direction based on substrate layers and slope (Ozkul et al., 2013). Notice however that we have to rely on 2D observations on wall surfaces present in the quarry, which do not allow a full 3D reconstruction of the paleoflow directions.

In Unit 1 fenestral-like porosity (see Figs. 9A and B), along with evidence of brecciation supports a system with stagnant and shallow water, attributed to a marsh environment. A sharp boundary within the overlying non-travertine composite layer, interpreted as erosion surface occurring at the same elevation throughout the study area, indicates that the environment most likely consisted of a uniform, vast, extensive flat pool. Notice that this unit starts with vadose pisoids and brecciation structures and progressively changes to clotted micrite similarly to other reported lacustrine examples (e.g. Arenas et al., 1997; Alonso-Zarza and Wright, 2015). This unit ended with an unconsolidated thick non-travertine deposits, which reflects an interruption of the spring activity. Unit 1 is relatively poor in shrubs and where they occur, they consist of pustular shrubs. This points to low energy water-flow resulting from remoteness of the main spring and/or different fluid. This is in line with the $\delta^{13}C$ values being relatively more enriched in comparison with Unit 2 and 3. In fact, evasion of CO_2 has yielded a remarkable increase in the heavy carbon isotopes, and as a consequence the $\delta^{13}C$ gets the highest amount at the furthest distance from the springs (Fouke, 2000, 2011; Kele et al., 2011). Therefore, the decreasing trend in the $\delta^{13}C$ from Unit 1 to Unit 3 indicates a possible evolution of the succession from distal areas (Unit 1) to more proximal (Unit 3) and ultimately in the direct vicinity of the original thermal springs.

Unit 2 is marked by wavy laminations of alternating dendritic shrubs (individual thickness of 1 to 5 cm) and thin micritic laminae (5 mm mean thickness) making up wavy crust structures, making up a slightly inclined micro-terraced system with shrub flats. The latter flats, however, gradually transit laterally in downflow direction, into straight layers, which are reflecting a marshy environment. This environment is dominantly sub-aqueous, i.e. lacustrine, but it became occasionally sub-aerially exposed in marginal parts reflecting palustrine conditions with in-situ reed development. According to Freytet and Verrecchia (2002), hydrophilic plants colonization marks especially newly established palustrine settings which argue for more remoter location from the main feeder spring(s) in comparison to the shrub flat. Furthermore, the development of shrub structures, in general, requires higher energy levels and thus more proximity to spring(s) than those of lithotypes assigned to the marsh environments (e.g. mudstone).

The shrub flat deposits are characterised by layers including an alternation of shrub micrite and porous micritic layers with fenestral porosity, reflecting seasonal variations during their development (Pentecost, 2005; Jones and Renaut, 2010; Wang et al., 2016). The less turbulent water flow during cold seasons most likely resulted in the development of the porous micritic layers. The shrub micrite structures likely formed during warm seasons, as also was proposed by Wang et al. (2016). Such seasonal variation is in agreement with the stable isotope and pollen analyses reported by Toker et al. (2015). The results obtained by the latter authors reflect alternating warm summer and cold and wet winter seasons when this travertine formed (Late Pleistocene). Accordingly, it can be interpreted that thick laminae of dendritic shrubs formed during warm seasons with high energy water-flow conditions, which caused rapid CO_2 degassing. Indeed, the study area occurs at a mean elevation of 550 m, likely to have snow-cover in winter-time. Generally, during cold seasons, springs especially in pool environments were covered by snow and ice, which could reduce CO_2 degassing. At the top of Unit 2 sub-aerial exposure features occur (see Fig. 8G), such as red-stained layer from oxidation of iron components and reflecting periodic interruption of travertine precipitation.

Unit 3 is characterised by an alternation of deposits reflecting a faint low angle terrace slope to smooth slope facies in downslope direction. The latter facies represents the shrub and dominantly marsh environment. In the slope facies, reeds were growing in small pools, at the end of the slope where the water was slowing down, lowering the water turbulence. The terrace slope facies, generally, reflects a high energy, turbulent water flow, which is expected to be situated closer to the feeder spring(s). The presence of this facies within Unit 3 supports its relative proximity to the spring(s) in comparison to Unit 1 and 2. Moreover, the relatively depleted $\delta^{13}C$ values are in agreement with rapid water flow and occurrence of CO_2 degassing. Finally, it should be noted that in all the three studied units, the lithotypes attributed to the dynamically high and low energy flow exists within the central and peripheral parts, respectively.

8.4 Diagenetic history and development of porosity

The studied deposits are relatively young, since they are Pleistocene in age, and have never been deeply buried. Therefore, burial diagenetic processes can be excluded. However, widespread alteration reveals the influence of early diagenetic processes, most likely due to the passage of thermogene and meteoric waters during ongoing travertine formation.

On macroscopic scale, the most obvious alteration results in dissolution enlarged cavities and plant decay. They are mainly observed above the non-travertine deposits in reed lithotype and cut the horizontal lamination. Their occurrence in travertines, formed in the more distal parts away from the springs, is probably related to an increased influence of meteoric water infiltration. However, regarding the hydrothermal fluid system characteristics, it cannot be excluded that some aggressive acidic fluids as for example H_2S-bearing fluids could have caused such type of enlargements. However, no reaction products like gypsum have been encountered. Another eye-catching type of porosity in the field is the well-developed fenestral-like porosity, the origin of which is attributed to organic decay (Chafetz, 2013). Another type of porosity relates to leaching of the unstable part of shells during diagenesis giving rise to bio-moldic porosity development (Flügel, 2010). Vuggy porosity is widespread, which originates from enlargement of other types of porosity. Framework porosity is well developed in dendritic shrubs and to a lesser extent in radial shrubs. In pustular shrubs, intergranular porosity is the only pore type, which is usually primary. SEM analyses and fluorescence microscopy also reveal microporosity in most of the studied lithologies.

Recrystallization of micrite manifesting aggradational neomorphism (Love and Chafetz, 1988) is often observed. One of the most important diagenetic processes is cementation in the form of fibrous cement rims, bladed cements and dogtooth cements. They grow perpendicular on pre-existing components and surround them isopachously. According to Claes et al. (2017), their origin can be related to subsurface water percolation in travertine systems. The occurrence of equant mosaic cement and blocky cement filling cavities among the components was also reported by Rainey and Jones (2007) from the Holocene tufa deposits of Fall Creek (Canada). They reported that adjacent sub-crystals use each other as growth template and therefore appear as a parallel overprinting of trigonal crystals. Claes et al. (2017) addressed the rounded edges of the cements and related them to late-stage dissolution. Alternation of light-coloured crystals and dark-coloured micrite forms isopachous banded crystal - micrite couplets. They are usually found around degraded, probably biologically induced, clotted micrite. Dripstone cements exhibit gravitational textures indicating vadose meteoric diagenesis. Fan-shaped clotted micrite, which probably originated from cyanobacteria and which show dull luminescence, can be interpreted as recrystallization products based on existing ghost textures of primary micrite. Undulose extinction, which sometimes is observed, shows signs of extensive recrystallization. Bioturbated intervals were more susceptible to diagenesis, as inferred from the higher contribution of microporosity and associated wispy luminescence (see Fig. 10O) of these intervals. The presence of Fe-Mn-oxide/hydroxide dendrites is consistent with oxidation conditions during sub-areal exposure right after sedimentation.

5. Conclusion

The current study documents the dominantly subaqueous depositional system that prevailed at the beginning of the development in the Ballik travertines mainly consists of deposits that accumulated in shrub flat and marshy environments with some micro-terracette morphologies. These sub-horizontal travertines from the Çakmak quarry in the Denizli Basin represent palustrine and lacustrine environmental conditions. The lithotypes testify of changing water flow conditions, quiescence and erosional processes. The lithotype analysis reveals that reworked material of formerly precipitated travertine and abiotic as well as biologically in-place precipitation played an important role in the formation of the sub-horizontal strata. The small-scale variations in depositional environment are reflected by lateral and vertical variations in lithotype distribution. Dendritic shrubs are the dominant lithotype of the shrub flat environment. Spongy microbial, clotted micrite and radial shrubs are usually associated with bioclastic ostracod and gastropod deposits, and thus indicate pond to lacustrine conditions with microbial influence. Reed in association with grass and mudstone lithotypes characterise palustrine depositional environments. They often occur adjacent to non-travertine deposits and reflect more stagnant water conditions. Peloidal lithotype can be found in both marsh and shrub flat environments. Granular pisoid and oncoid fabrics are related to the edge of ponds. Detrital input is demonstrated by the (limited) presence of quartz and clay minerals, best developed in non-travertine deposits, which are rather exceptional in their appearance, but which mark the boundaries between the units studied. Existence of non-carbonate phases is also reflected in the trace elemental composition, more specifically in the elements grouping Al, Fe, Mn, K, P and Ti. Moreover, this study clearly reveals important interference of early diagenetic processes like cementation and dissolution. In terms of porosity, primary (intergranular and framework) and secondary porosity (connected and disconnected vuggy, mouldic, framework, fractures, and microporosity) characterize the travertines both on the macro- and micro-scale. Results of carbon and oxygen stable isotope and geochemical element analysis reflect small-scale variations in sedimentary and diagenetic alteration. The small-scale differences between cement and micrite stable C- and O-isotope patterns in Unit 1 are interpreted to reflect the influence of infiltrating meteoric water and the reverse behaviour in Unit 2 can be temperature related caused by the extra discharge infiltration through the basin floor of which the uppermost layers became indurated. However, the non-systematic behaviour of the isotopic patterns of micrite and cement in Unit 3 is interpreted by mixing of waters of different origins. Finally, the co-variation of Mg, Na, S, Ba and Sr point towards subsurface water/rock interactions likely involving Triassic evaporitic carbonates of the Lycian nappe affecting the fluids that later were involved in carbonate precipitation.

Acknowledgements

The authors are grateful to Prof. Dr. S. Bouillon and colleagues of Department of Earth and Environmental Sciences of the KU Leuven (Belgium) for performing the oxygen and carbon stable isotope measurements. Prof. Dr. M. Özkul and Dr. M. Erthal are thanked for their help during fieldwork. H. Nijs is acknowledged for the careful preparation of thin sections and Dr. E. Vassilieva for the ICP-OES analysis. This work was supported by KU Leuven research and development.

Appendices

Additional Supporting Information of stable isotope analysis and elemental composition of different lithotypes can be found as Appendix 1 and 2 in the online version of this article.

References

Alçiçek, H., Varol, B., Özkul, M., 2007. Sedimentary facies, depositional environments and palaeogeographic evolution of the Neogene Denizli Basin, SW Anatolia, Turkey. Sedimentary Geology, 202, 596–637.

Alçiçek, H., 2010. Stratigraphic correlation of the Neogene basins in southwestern Anatolia: Regional palaeogeographical, palaeoclimatic and tectonic implications. Palaeogeography, Palaeoclimatology, Palaeoecology 291, 297–318.

Alçiçek, H., Bülbül, A., Yavuzer, İ., Alçiçek, C., 2018. Origin and evolution of the thermal waters from the Pamukkale Geothermal Field (Denizli Basin, SW Anatolia, Turkey): Insights from hydrogeochemistry and geothermometry. Volcanology and Geothermal Research, In Press.

Alçiçek, M.C., Brogi, A., Capezzuoli, E., Liotta, D., Meccheri, M., 2013. Superimposed basins formation during the Neogene–Quaternary extensional tectonics in SW-Anatolia (Turkey): insights from the kinematics of the Dinar Fault Zone. Tectonophysics 608, 713–727.

Alonso-Zarza, A.M., Wright, P., 2010. Palustrine carbonates. In: Alonso-Zarza, A.M., Tanner, L.H. (Eds.), Carbonates in Continental Settings. Development in Sedimentology, Elsevier Amsterdam, 61, pp. 225–267.

Altunel, E. and Hancock, P.L., 1993a. Active fissuring, faulting and travertine deposition at Pamukkale (W Turkey).In: Neotectonics and Active Faulting (edited by I.S. Stewart, C.Vita-Finzi & L.A Owen). Zeitschrift fur Geomorfologie Supply. Vol., 94, 285-302.

Altunel, E. and Hancock, P.L., 1993b. Morphological features and tectonic setting of Quaternary travertines at Pamukkale, western Turkey. Geological Journal, 28, 335-346.

Altunel, E. 1994, Active Tectonics and Evolution of Quaternary Travertines at Pamukkale, Western Turkey. Unpublished, Ph.D.thesis, University of Bristol, U.K.

Altunel, E. and Hancock, P.L., 1996. Structural attributes of travertine-filled extensional fissures in the Pamukkale Plateau, Western Turkey. Int.Geol.Review, 38, 8, 768-777.

Andrews, J.E., Riding, R., Dennis, P.F., 1993. Stable isotopic compositions of recent freshwater cyanobacterial carbonates from the British Isles: local and regional environmental controls. Sedimentology, 40, 303–314.

Andrews, J. E., Greenaway, A. M., Dennis, P. F., 1998. Combined carbon isotope and C/N ratios as indicators of source and fate of organic matter in a poorly flushed, tropical estuary: Hunts Bay, Kingston Harbour, Jamaica. Estuarine, Coastal and Shelf Science, 46(5), 743–756.

Andrews, J.E., Riding, R., 2001. Depositional facies and aqueous-solid geochemistry of travertine-depositing hot springs (Angel Terrace, Mammoth Hot Springs, Yellowstone National Park, U.S.A.) – Discussion. Sedimentary Research, 71, 496–497.

Arenas, C., Casanova, J., Pardo, G., 1997. Stable isotope characterization of the Miocene lacustrine systems of Los Monegros (Ebro Basin, Spain): palaeogeographic and palaeoclimatic implications. Palaeogeography, Palaeoclimatology, Palaeoecology, 129, 133-155.

Arenas, C., GutiÉrrez, F., OsÁcar, C., Sancho., C., 2000. Sedimentology and geochemistry of fluvio-lacustrine tufa deposits controlled by evaporite solution subsidence in the central Ebro Depression, NE Spain. Sedimentology, 47, 993–909.

Arenas, C., Cabrera, L., Ramos, E., 2007. Sedimentology of tufa facies and continental microbialites from the Palaeogene of Mallorca Island (Spain). Sedimentary Geology, 197, 1–27.

Arenas, C., Vàzquez-Urbez, M., Auqué, L., Sancho, C., Osàcar, C., Pardo, G., 2014. Intrinsic and extrinsic controls of spatial and temporal variations in modern fluvial tufa sedimentation: a thirteen-year record from a semi-arid environment. Sedimentology, 61, 90–132.

Barilaro, F., Della Porta, G., Capezuoli, E., 2012. Depositional geometry and fabric types of hydrothermal travertine deposits (Albegna Valley, Tuscany, Italy). Rendiconti Online Società Geologica Italiana, 21, 1024–1025.

Bianchi, T.S., 2007. Biogeochemistry of Estuaries. Oxford University Press, Inc. 696 pp.

Brogi, A., Capezzuoli, E., 2009. Travertine deposition and faulting: The fault-related travertine fissure-ridge at Terme S. Giovanni, Rapolano Terme (Italy). Geologische Rundschau, 98, 931–947.

Brogi, A., Capezzuoli, E., 2014. Earthquake impact on fissure-ridge type travertine deposition.

Geological Magazine, 151, 1135–1143.

Buczynski, C., Chafetz, H. S., 1991. Habit of bacterially induced precipitates of calcium carbonate and the influence of medium viscosity on mineralogy: Journal of Sedimentary Research, 61, 226–233.

Carminatti, M., Wolff, B., Gamboa, L., 2009. New exploratory frontiers in Brazil. In: 19th World Petroleum Congress. World Petroleum Council.

Capezzuoli, E., Gandin, A., Pedley, M., 2014. Decoding tufa and travertine (fresh water carbonates) in the sedimentary record: the state of the art. Sedimentology, 61, 1–21.

Choquette, P. W., Pray, L. C., 1970. Geologic nomenclature and classification of porosity in sedimentary carbonates. American Association of Petroleum Geologists Bulletin, 54, 207–244.

Chafetz, H.S., Folk R.L., 1984. Travertines: Depositional morphology and the bacterially-constructed constituents. Sedimentary Petrology, 54, 299−316.

Chafetz, H.S., 1996. Marine peloids; a product of bacterially induced precipitation of calcite. Sedimentary Petrology, 56, 912-917.

Chafetz, H.S., Guidry, S.A., 1999. Bacterial shrubs, crystal shrubs, and ray-crystal shrubs: bacterial vs. abiotic precipitation. Sedimentary Geology, 126, 57–74.

Chafetz, H. S., 2013. Porosity in bacterially induced carbonates: Focus on micropores. American Association of Petroleum Geologists Bulletin, 97, 2103–2111.

Claes, H., Soete, J., Van Noten, K., El Desouky, H., Erthal, M. M., Vanhaecke, F., Özkul, M., Swennen, R., 2015. Sedimentology, three-dimensional geobody reconstruction and carbon dioxide origin of Pleistocene travertine deposits in the Ballık area (south-west Turkey). Sedimentology, 62, 1409-1445.

Claes, H., Marques Erthal, M., Soete, J., Özkul, M., Swennen, R., 2017. Shrub and pore type classification: Petrography of travertine shrubs from the Ballık-Belevi area (Denizli, SW Turkey). Quaternary International, 437, 147–163.

Croci, A., Della Porta, G., Capezzuoli, E., 2016. Depositional architecture of a mixed travertine-terrigenous system in a fault-controlled continental extensional basin (Messinian, Southern Tuscany, Central Italy). Sedimentary Geology, 332, 13–39.

De Boever, E., Foubert, A., Lopez, B., Swennen, R., Jaworowski, C., Özkul, M., Virgone, A., 2016. Comparative study of the Pleistocene Cakmak quarry (Denizli Basin, Turkey) and modern Mammoth Hot Springs deposits (Yellowstone National Park, USA). Quaternary International, 437, 129–146.

Della Porta, G., 2015. Carbonate build-ups in lacustrine, hydrothermal and fluvial settings: comparing depositional geometry, fabric types and geochemical signature. Microbial Carbonates in Space and Time: Implications for Global Exploration and Production. Geological Society, London, Special Publications, 418, 17–68.

Dias, J. L., 1998. Analise sedimentológica e estratigráfica do Andar Aptiano em parte da margem leste do Brasil e no platô das Malvinas - consideraçoes sobre as primeiras incursões e ingressões marinhas do Oceano Atlântico sul Meridional: Universidade federal do Rio Grande Do Sul, 399.

Dias, J. L., 2005). Tectônica, estratigrafia e sedimentação no Andar Aptiano da margem leste brasileira. Boletim de Geociências da Petrobras, 13, 7–25.

Dunham, R.J., 1962. Classification of carbonate rocks according to depositional texture. - In: Ham, W.E. (Eds.), Classification of Carbonate Rocks. American Association of Petroleum Geologists, Tulsa, Oklahoma, Memoirs, 1, pp. 108–121.

Dupraz, C., Visscher, P. T., Baumgartner, L. K., Reid, R. P., 2004. Microbe-mineral interactions: Early carbonate precipitation in a hypersaline lake (Eleuthera Island, Bahamas). Sedimentology, 51, 745–765.

Dupraz, C., Reid, R. P., Braissant, O., Decho, A. W., Norman, R. S., Visscher, P. T., 2009. Processes of carbonate precipitation in modern microbial mats. Earth-Science Reviews, 96, 141–162.

El Desouky, H., Soete, J., Claes, H., Özkul, M., Vanhaecke, F., Swennen, R., 2015. Novel applications of fluid inclusions and isotope geochemistry in unravelling the genesis of fossil travertine systems. Sedimentology, 62, 27–56.

Embry, A.F., Klovan, S.E., 1971. A late Devonian reef tract on North-eastern Banks Island, N.W.T. Bulletin of Canadian Petroleum Geology, 19, 730–791.

Erthal, M. M., Capezzuoli, E., Mancini, A., Claes, H., Soete, J., Swennen, R., 2017. Shrub morpho-types as indicator for the water flow energy - Tivoli travertine case (Central Italy). Sedimentary Geology, 347, 79–99.

Faccenna, C., Soligo, M., Billi, A., De Filippis, L., Funiciello, R., Rossetti, C., Tuccimei, P., 2009. Late Pleistocene depositional cycles of the Lapis Tiburtinus travertine (Tivoli, Central Italy): possible influence of climate and fault activity. Global and Planetary Change, 63, 299–309.

Flügel, E., 2010. Microfacies of carbonate rocks. Second edition, Springer-Verlag, 994.

Folk, R.L. Chafetz, H.S., 1983. Pisoliths (pisoids) in Quaternary travertines of Tivoli, Italy. In: Peryt, T.M. (Ed.s), Coated Grains. Springer-Verlag, Berlin, pp. 474–487.

Fouke, B.W., Farmer, J.D., Des Marais, D.D., Pratt, L., Sturchio, N.C., Burns, P.C., Discipulo, M.K., 2000. Depositional facies and aqueous-solid geochemistry of travertine depositing hot springs (Angel Terrace, Mammoth Hot Springs, Yellowstone National Park, U.S.A.). Journal of Sedimentary Research, 70, 565–595.

Fouke, B.W., 2011. Hot-spring Geobiology: abiotic and biotic influence on travertine formation at Mammoth Hot Springs, Yellowstone National Park, USA. Sedimentology, 59, 170–219.

Freytet, P., Verrecchia, E.P., 2002. Lacustrine and palustrine carbonate petrography: An overview. Journal of Paleolimnology, 27(2), 221–237.

Freytet, P., Plet, A., 1996. Modern freshwater microbial carbonates: the Phormidium stromatolites (tufa-travertine) of Southeastern Burgundy (Paris Basin, France). Facies, 5, 219–237.

Gandin, A., Capezzuoli, E., 2008. Travertine versus Calcareous tufa: distinctive petrologic features and related stable isotopes signature. Il Quaternario, 21, 125–136.

Gandin, A., Capezzuoli, E., 2014. Travertine: Distinctive depositional fabrics of carbonates from thermal spring systems. Sedimentology, 61, 264-290.

Gierlowski-Kordesch, E. H., 2010. Lacustrine carbonates. In: Alonso-Zarza, A. M., Tanner, L. H. (Eds.), Carbonates in Continental Settings: Facies, Environments and Processes. Developments in Sedimentology, Elsevier, Amsterdam, 61, pp. 1–101.

Golubic, S., Violante, C., Plenkovic-Moraj, A. and Grgasovic, T., 2009. Travertines and calcareous tufa deposits: an insight into diagenesis. Geologia, Croatia, 61, 363–379.

Guo, L., Riding, R., 1992. Aragonite laminae in hot water travertine crusts, Rapolano Terme, Italy. Sedimentology, 39, 1067–1079.

Guo, L., Riding, R., 1998. Hot-spring travertine facies and sequences, Late Pleistocene, Rapolano Terme, Italy. Sedimentology, 45, 163–190.

Guo, L., Riding, R., 1999. Rapid facies changes in Holocene fissure ridge hot spring travertines, Rapolano Terme , Italy. Sedimentology, 46, 1145–1158.

Gürbüz, A., Boyraz, S., Ismael, M.T., 2012. Plio-Quaternary development of the Baklan– Dinar graben: implications for cross-graben formation in SW Turkey. International Geology Review, 54, 33–50.

Hancock, P.L., Chalmers, R.M.L., Altunel, E. ve Çakır, Z., 1999. Travitonics: using travertines in active fault studies. Journal of Structural Geology, 21, 903-916.

Hayes, J.M., 2001. Fractionation of carbon and hydrogen isotopes in biosynthetic processes. Reviews in Mineralogy and Geochemistry, 43, 225-279.

Jones, B., Renaut, R.W., 2010. Calcareous spring deposits in continental settings. In: Alonso-Zarza, A.M., Tanner, L.H. (Eds.), Carbonates in Continental Settings. Developments in Sedimentology, Elsevier, Amsterdam, 61, pp. 177–224.

Kele, S., Demény, A., Siklósy, Z., Németh, T., Tóth, M., Kovács, M.B., 2008. Chemical and stable isotope composition of recent hot-water travertines and associated thermal waters, from Egerszalók, Hungary: Depositional facies and non-equilibrium fractionation.

Sedimentary Geology, 211, 53–72.

Kele S., Özkul M., Fórizs I., Gökgöz A., Baykara M. O., Alçiçek M. C., Németh T., 2011. Stable isotope geochemical study of Pamukkale travertines: New evidences of low-temperature non-equilibrium calcite-water fractionation. Sedimentary Geology, 239, 191–212.

Koçyiğit, A., 2005. The Denizli graben-horst system and the eastern limit of western Anatolian continental extension: basin fill, structure, deformational mode, throw amount and episodic evolutionary history, SW Turkey. Geodinamica Acta, 18, 167–208.

Krumbein, W. E., Cohen, Y., Shilo, M., 1977. Solar Lake (Sinai): 4. Stromatolitic cyanobacterial mats: Limnology and Oceanography, 22, 635–656.

Love, K. M., Chafetz, H. S., 1988. Diagenesis of laminated travertine crusts, Arbuckle Mountains, Oklahoma. Journal of Sedimentary Research, 58(3), 441–445.

Meyers, P.A., 1994. Preservation of source identification of sedimentary organic matter during and after deposition. Chemical Geology, 144, 299–302.

Meyers, P.A., Takemura, K., 1997. Quaternary changes in delivery and accumulation of organic matter in sediments of Lake Biwa, Japan. Paleolimnology, 19, 211–219.

Mesci, B.L., Gursoy, H., Tatar, O., 2008. The evolution of travertine masses in the Sivas Area (Central Turkey) and their relationships to active tectonics. Turkish Journal of Earth Sciences, 17, 219–240.

Monty, C.L.V., 1976. The origin and development of crypalgal fabric. In: Stromatolites (Ed. by M. R. Walter), Elsevier Amsterdam, Development in Sedimentology, 20, 193–249.

Özkul, M., Varol, B., Alçiçek, M.C., 2002. Depositional environments and petrography of

Denizli travertines. Bulletin of the Mineral Research and Exploration (MTA Bulletin), 125, 13–29.

Özkul, M., Kele, S., Gökgöz, A., Shen, C.C., Jones, B., Baykara, M.O., Fórizs, I., Németh, T., Chang, Y.-W., Alçiçek, M.C., 2013. Comparison of the Quaternary travertine sites in the Denizli Extensional Basin based on their depositional and geochemical data. Sedimentary Geology, 294, 179–204.

Özkul, M., Gökgöz, A., Kele, S., Baykara, M.O., Shen, C.-C., Chang, Y.-W., Kaya, A., Hançer, M., Aratman, C., Akın, T., Örü, Z., 2014. Sedimentological and geochemical characteristics of a fluvial travertine: a case from the eastern Mediterranean region. Sedimentology, 61, 291−319.

Pentecost, A., 2005. Travertine. Springer-Verlag, Berlin Heidelberg. 445 pp.

Rainey, D.K., Jones, B., 2007. Rapid cold water formation and recrystallization of relict bryophyte tufa at the Fall Creek cold springs, Alberta, Canada. Canadian Journal of Earth Sciences, 44, 999–909.

Rainey, D. K., Jones, B., 2009. Abiotic versus biotic controls on the development of the Fairmont Hot Springs carbonate deposit, British Columbia, Canada: Sedimentology, 56, 1932–1957.

Rezende, M. F., Pope, M. C., 2015. Importance of depositional texture in pore characterization of subsalt microbialite carbonates, offshore Brazil. Geological Society, London, Special Publications, 419.

Rice, D. L., Hanson, R. B., 1984. A kinetic model for detritus nitrogen: role of the associated bacteria in nitrogen accumulation. Bulletin of Marine Science, 35, 326-340.

Riding, R., 2006. Microbial carbonates: the geological record of calcified bacterial-algal mats and biofilms. Sedimentology, 47, (Suppl.1), 179−214.

Ronchi, P., Cruciani, F., 2015. Continental carbonates as hydrocarbon reservoir, an analogue case study from the travertine of Saturnia, Italy. AAPG Bulletin, 99, 711–734.

Saller, A., Rushton, S., Buambua, L., Inman, K., McNeil, R., Dickson, J. A. D., 2016. Presalt stratigraphy and depositional system in the Kwanza Basin, offshore Angola. AAPG Bulletin, 100, 1135 – 1164.

Sant'Anna, L.G., Riccomini, C., Rodrigues- Francisco, B.H., Sial, A.N., Carvalho, M.D., Moura, C.A.V., 2004. The Palaeocene travertine system of the Itaboraí basin, Southeastern Brazil. Journal of South American Earth Sciences, 18, 11−25.

Schröder, S., Ibekwe, A., Saunders, M., Dixon, R. Fisher, A., 2016. Algal – microbial carbonates of the Namibe Basin (Albian , Angola): implications for microbial carbonate mound development in the South Atlantic Legend. Petroleum Geoscience, 22, 71–90.

Sözbilir, H., 2005. Oligo-Miocene extension in the Lycian orogen: evidence from the Lycian molasse basin, SW Turkey. Geodinamica Acta, 19, 255−292.

Soete, J., Kleipool, L.M., Claes, H., Claes, S., Hamaekers, H., Kele, S., Özkul, M., Foubert, A., Reijmer, J.J.G., Swennen, R., 2015. Acoustic properties in travertines and their relation to porosity and pore types. Marine and Petroleum Geology, 59, 320-335.

Soete, J., Claes, S., Claes, H., Janssens, N., Cnudde, V., Huysmans, M., Swennen, R., 2017. Lattice Boltzmann simulations of fluid flow in continental carbonate reservoir rocks and in upscaled rock models generated with multiple-point geostatistics. Geofluids, 2017, 24.

Teboul, P. A., Durlet, C., Gaucher, E. C., Virgone, A., Girard, J. P., Curie, J., Camoin, G. F., 2016. Origins of elements building travertine and tufa: New perspectives provided by isotopic and geochemical tracers. Sedimentary Geology, 334, 97–114.

Thornton, S. F., McManus, J., 1994. Application of organic carbon and nitrogen stable isotope and C/N ratios as source indicators of organic matter provenance in estuarine systems: evidence from the Tay Estuary, Scotland. Estuarine, Coastal and Shelf Science 39, 219–233.

Toker, E., Kayseri-Özer, M.S., Özkul, M., Kele, S., 2015. Depositional system and palaeoclimatic interpretations of Middle to Late Pleistocene travertines: Kocabaş, Denizli, south-west Turkey. Sedimentology, 62, 5, 1360-1383.

Van Hinsbergen, D.J.J., Kaymakci, N., Spakman, W., Torsvik, T.H., 2010. Reconciling the geological history of western Turkey with plate circuits and mantle tomography. Earth and Planetary Science Letters, 297, 674–696.

Van Noten, K., Claes, H., Soete, J., Foubert, A., Özkul, M., Swennen, R., 2013. Fracture networks and strike-slip deformation along reactivated normal faults in Quaternary travertine deposits, Denizli Basin, western Turkey. Tectonophysics, 599, 154–170.

Vasconcelos, C., McKenzie, J.A., 1997. Microbial mediation of modern dolomite precipitation and diagenesis under anoxic conditions (Lagoa Vermelha, Rio de Janeiro, Brazil). Journal of Sedimentary Research, 67, 379–390.

Vasconcelos, C., McKenzie, J.A., 1997. Microbial mediation of modern dolomite precipitation and diagenesis under anoxic conditions (Lagoa Vermelha, Rio de Janeiro, Brazil). Journal of Sedimentary Research 67, 378–390.

Verbiest, M., Soete, J., Fay-Gomord, O., Adriaens, R., Aratman, C., Swennen, R., 2018. Detrital deposits near the Ballık travertine analogue (SW Turkey): Insights from petrographical and mineralogical analyses. Submitted to Sedimentary Geology.

Wang, H., Yan, H., Liu, Z., 2014. Contrasts in variations of the carbon and oxygen isotopic composition of travertines formed in pools and a ramp stream at Huanglong ravine, China: implications for paleoclimatic interpretations. Chemical Geology, 125, 34–48.

Wang, Z., Meyer, M. C., Hoffmann, D. L., 2016. Sedimentology, petrography and early diagenesis of a travertine–colluvium succession from Chusang (southern Tibet). Sedimentary Geology, 342, 218–236.

Westaway, R., 1993. Neogene evolution of the Denizli region of western Turkey. Structural Geology, 15, 37–53.

Westaway, R., Guillou, H., Yurtmen, S., Demir, T., Scaillet, S., Rowbotham, G., 2005 Investigation of the conditions at the start of the present phase of crustal extension in western Turkey, from observations in and around the Denizli region. Geodinamica Acta, 19, 209–239.

Wright, V. P., 2012. Lacustrine carbonates in rift settings: the interaction of volcanic and microbial processes on carbonate deposition: Geological Society, London, Special Publications, 370, 39–47.

Wright, V.P., Barnett, A.J., 2015. An abiotic model for the development of textures in some

South Atlantic early Cretaceous lacustrine carbonates Cretaceous (part). In: Microbial Carbonates in Space and Time: Implications for Global Exploration and Production, p. 418.

Yan, H., Sun, H., Liu, Z., 2012. Equilibrium vs. kinetic fractionation of oxygen isotopes in the two low-temperature travertine-depositing systems with distinct hydrodynamic conditions at Baishuitai, Yunnan SW China. Chemical Geology, 95, 63–78.

Lithotypes name	Description on macroscopic scale	Description on microscopic scale	Interpretation	Reference	Distribution, lateral continuation and associated lithotypes
L1: Dendritic shrub	Undulating layers of bright white to creamy travertine, with regular geometric	Bush-like structures with dendritic outlines of fibrous (Figs. 7A, B) and wide dendritic	The shrubs are laterally persistent in wavy crust structures making up almost straight to slightly inclined layers, pointing to deposition in gently	(Guo and Riding, 1992, 1999; Folk	In unit 2 and 3 they can be followed laterally and vertically over more than 100

Table caption

Table 1. Description and interpretation of travertine lithotypes recognized in the studied succession.

Table 2. TOC, C/N and organic carbon isotope values of organic matter of the different lithotypes in Çakmak Quarry.

Table

boundstone	arborescent and arbustiform shrub morphologies. Thickness of the individual shrub crusts changes from 5 mm to 2 cm (Figs. 6A, B, C).	structures (Figs. 7C, D) diverging away from a central region with nucleation center (Fig. 7E). These rims are up to 1–2 cm in length and 2–5 cm in width. The dendritic fabrics occur adjacent to each other, as dense and tightly packed clotted structures.	sloping micro-terraced settings. Some lateral variations have been noticed where the branch morphology of dendritic shrubs changed from narrow and elongated to wider and shorter widespread morphotypes often with interdigitated pore shapes (Fig 7.B to F) pointing to hydrodynamic conditions (as stated by Erthal et al., 2017) and pre-existing small-scale topography influence.	and Chafetz, 1983; Chafetz and Guidry, 1999; Chafetz, 2013).	m and 8 m, respectively. However, it appears partially to rarely in discontinuous layers in unit 1. Associated lithotypes are L4, L8, L7
L2: Pustular shrub grainstone	White, tightly cemented, sub-rounded shrubs relatively homogeneous in morphology and varying from 0.1 to 4 mm in size (Fig. 6F).	Densely packed micritic clumps with uniform internal structure (Fig. 7G). Their limited size points to their stunted growth origin, compared to dendritic shrubs.	Good sorting, but lacking of roundness point that the formation of pustular shrubs probably took place after decrease in turbulence in a water column where they accumulated and made up lenticular bodies at the bottom and behind obstacles. It indicates lacustrine marshy environments and distal parts of shrub flats.	(Claes et al., 2016).	It shows extensive distribution over entire setting but discontinuously as stucking layer between other. Associated lithotypes is L1
L3: Radial shrub packstone/grainstone	Spherical and rounded to sub-spherical to sub-rounded white colored grains, 1 to 5 mm in size (Fig. 6G).	Iirregular to regular concentric radial morphology that develops around a nucleus, which appears alongside clotted peloids floating in a microsparitic matrix (Fig. 7H and I). The central cores in some cases are partially dissolved.	Their rounded shape with internal radial branches point towards small shallow ponds as depositional setting. This lithotype usually develops in the lower part of shrub flats and marsh settings. An organic influence on the generation of the internal radially structured features is supported by the abundance of bacterial-like coccoid structures.	Rainey and Jones (2009), Della Porta (2015) and Croci et al. (2016).	It discontinuously occurs in the distal depositional setting in the three units, in horizontal lenses of 10 to 60 cm in thickness and up to 60 cm in width. Associated lithotypes is L6
L4: Peloidal packstone	Beige colour with fenestral-like pores that accentuate the horizontal lamination (Figs. 8A and B).	Micritic clumps, with limited microbial filaments (white colour) or dark coloured peloids floating in a sparitic or micro-sparitic matrix (Fig. 9A and B).	The depositional environment corresponds to a shrub flat (in situ formation) and marsh-pool environment (reworked peloids), specially the edge of shrub flats as they usually form where shrub layers disappear. Dark and light colour can be related to high and low quantities of organic matter, respectively.	(Claes et al., 2015)	Lateral continuousover 200 m in length and 2 m in thickness. Associated lithotypes are L1, L2, L8
L5: Coated-grain grainstone to packstone	Dark colored layers of spherical to ellipsoidal coated grains ranging from fine to coarse sand sized. The coated grains are glued together by cementation (Fig. 8D).	Consisting of peloids, pisoids, oncoids, intraclasts, and coated bubbles floating in silt-sized micrite matrix. Pisoids of crinkled and irregular grains up to 5 mm in size are the most abundant components (Fig. 9C). Intraclasts are observed as millimetric-size breccia-like fragments.	Co-occurrence of carbonate grains (peloids, ooids, pisoids and oncoids; Dunham, 1962) with phytoclastic and meniscus cement, pointing toward distal parts of a marsh environment, with evidence of calcification in a palustrine environment. The development of this lithotype can occur under vadose-like conditions in side-embayments of ponds during low-energy episodes in marshy environments.	Folk and Chafetz (1983), Guo and Riding (1999), Jones and Renaut (2010) and Özkul et al. (2014).	It appears in limited lateral continuous distal depositional settings (e.g away from the springs) of unit 2 and 3. Associated lithotypes are L6, L7
L6: Reed to grass rudstone to boundstone	Cream to white colored with imprints of up to 50 cm in diameter with reed and grass in growth position (boundstone) and fragments of spherical to ellipsoidal clasts (rudstone) up to 5 cm in size, i.e. hollow tubes, overgrown with calcite (Fig. 8 G and H).	They reveal a frame of calcite precipitation around phyto moldic pores (Fig. 9D). Skeletal fragments from ostracods and gastropods are observed.	It precipitated when sediments became trapped and lithified in the interstitial spaces between vascular plants (reeds and grass). Often associated with mudstone indicating paleoenvironmental conditions where waters cooled down sufficiently to allow plants to grow. This lithotype is found distally away from springs where the environment reflects palustrine conditions.	Guo and Riding (1999), Arenas et al. (2014), Özkul et al. (2014), Claes et al. (2015), Croci et al. (2016).	It laterally extends over several meters in distal settings of unit 2 and 3. They are frequently present above the marker horizon. Associated lithotypes are L5, L7, L8.
L7: Cryptalgal to bioclastic bioturbated silty mudstone	Dark to grey coloured dense and compact homogeneous micrite layers. In some cases patchy accumulations have been observed.	They are made up of silt-sized micritic aggregates (Fig. 9E), together with dispersed detrital quartz grains and clays, along with small amounts of organic matter such as twigs and plant stems, ostracods, gastropods, (with geopetal infill) (Fig. 11I), phytoclasts (like green algae) and locally accumulations of fecal pellets.	Strongly microbially affected since widespread ghost-structures of microbes like cyanobacteria have been noticed (see Figs. 9E). Whether the mud in this lithotype (Fig. 11K) formed by direct precipitation is unclear. The mud accumulations, however, support a low-energy environment with regular stagnant water pointing to a shallow palustrine to marshy environment. The bioturbated zones of the mudstones display more recrystallization, which may relate to the higher specific reaction surface or higher permeability affecting the infiltration of diagenetic solutions.	Guo and Riding (1999), Sant'Anna et al. (2004), Gierlowski-Kordesch (2010), Özkul et al. (2014), Gandin and Capezzuoli (2014)	Laterally continuous over several meters with cm to m thickness passing into phytoclastic lithotypes. It usually appears at the bottom of three units and rely together with patchy accumulations. Associated lithotypes are L5, L6, L8
L8: Clotted micrite packstone to boundstone	Compact gray-coloured travertines with layers that range from centimetres to metres in thickness.	They are made up of dense micrite referred to as "micrite islands" (sensu Riding, 2000). Clotted micrites are usually surrounded by bladed cement of 50–100 µm in length (Fig. 9F) which in some cases show mottled orange luminescence.	Microbially mediated precipitation with evidence of cyanobacteria, coccolith bacteria and algae making up homogeneous micrite points to an authigenic origin of the micrite clumps. They have rather large lateral extent and vertically they are often related to mudstone in lacustrine parts of marsh environments pointing to the same environment as mudstone.	Gierlowski-Kordesch, (2010), Gandin and Capezzuoli (2014)	Laterally continuous several meters in length with cm in thickness and laterally alternating with dendritic shrub and peloidal travertine. Associated lithotypes is L1
L9: Spongy boundstone	White porous sponge-like accumulations in patchy structures of several centimeters to a maximum of one meter in parallel layers (Fig. 8F).	They are composed of an intertwined network showing strong similarities to clotted and micritic clumps. However, their main characteristic relates to the widespread connected vuggy porosity (Fig. 9G), as well as macroscopic loose texture making up the spongy boundstone.	Large elongated filaments of, most likely, moss stems pointing to the relationship between plant-biomass and calcite encrustation, making up the spongy structures. Presence of spherical shapes in cross-section and tube shapes parallel to the structures support the existence of moss-like communities involved in the precipitation of this lithotype(Fig. 9H and I). They probably precipitated in shallow pan-shaped (Gandin and Capezzuoli, 2014) and/or non-quiescent marginal pool-type environments, where plants could accumulate behind the edge of a small pool, and where the water temperature became ambient.	Arenas et al. (2000, 2007) and Claes et al. (2016).	It shows patchy structures and laterally discontinuous layesr. It only occurs in unit 2. Associated lithotypes are L1, L8

Table 1

Samples	mg N	%N	%C	C/N	$\delta^{13}C_{OC}$ ‰	$\delta^{15}N$ ‰
fully cemented radial shrub	17	0.04	0.09	2.27	-19.1	1.0
radial shrub	17.7	0.05	0.15	3.44	-14.5	1.2
dendritic shrub	15.3	0.04	0.17	4.09	-23.4	2.1
dendritic shrub	17.6	0.04	0.14	3.97	-19.2	0.9
spongy	15.4	0.05	0.17	3.50	-23.2	1.6
peloid	17.4	0.04	0.14	4.04	-20.2	1.7
coated grain	17.9	0.05	0.21	4.60	-24.5	1.4
clotted micrite	17.9	0.05	0.17	3.32	-23.6	-0.1
pustular shrub	16.9	0.04	0.15	3.50	-23.9	1.3
pustular shrub	15.6	0.04	0.19	4.53	-22.7	0.9
mudstone	16.1	0.04	0.20	4.62	-24.6	0.9
reed	16.59	0.04	0.19	4.60	-23.9	3.4
reed	17.2	0.06	0.25	4.39	-22.6	2.0

Table 2

Figure captions

Fig. 1. Geological framework of the Denizli area (Turkey). A) Map of Turkey with indication of Denizli. B) Çakmak and adjacent quarry location in the Ballık domal area (google earth). C) Tectonic setting of the Denizli Basin with indication of the different Quaternary sub-basins. The star indicates the location of the Çakmak quarry (modified from Van Noten et al., 2013).

Fig. 2. (A and B): Overview of the studied units 1, 2 and 3 Units in the lower part of the Çakmak quarry (blue, red and pink lines). Lines show the lateral continuity of the travertine sub-horizontal laminites. (C) Shrub crust stacking pattern with intercalated porous micrite layers. (D) Close up view of intercalation of shrub crust and porous micritic laminates.

Fig. 3. (A) Schematic view of the Ballik travertines. Sequence 1: Sub-horizontal layered travertine (red box corresponds to study area). Sequence 2, 4 and 5: Major change towards non-travertine deposition with lacustrine marls (and fluvial conglomerates. Sequence 3: Continental carbonate in reed, smooth-sloping cascade and steep-sloping waterfall facies forming the domal travertines. Outline of this schematic view is based on data form Van Noten et al. (2013), Claes et al. (2015), and ongoing research of Verbiest et al., (under revision). (B) Overview image of the Çakmak quarry. (C) Line drawing of a southeast to northwest section of the Çakmak quarry, 65 m in height and ~400 m in width. The lowest part consists of the sub-horizontal facies (yellow colour) cut off by the smooth-sloping cascade (light blue colour) travertines that evolve into steeper waterfall systems (dark blue colour) and reed facies (green colour) (see Claes et al., 2015 and De Boever et al., 2016) (red box is a A). (D) 3D model of the Çakmak and Ilik quarry (red box is a B and C).

Fig. 4. Internal architecture patterns of the three travertine units identified in the sub-horizontal travertines in the Çakmak quarry. Unit 1 shows almost horizontal layering covered

by a non-travertine deposits dipping (10°) to E-SE. Unit 2 displays wavy lamination in the SE, which laterally evolves into flat horizontal layering to the NW. Unit 3 consists of slope layers in the SE, which laterally changes to horizontal layering in the NW. (A) Internal architecture patterns of Unit 1 showing almost horizontal layering covered by a non-travertine deposits (red colour) dipping (10°) to SE. Unit 2 displays wavy lamination in the SE, which laterally evolves into flat horizontal layering to the NW. This unit is overlain by an exposure surface (red line between Unit 2 and 3. Unit 3 consists of slope layers in the SE, which laterally changes to horizontal layering in the NW. (B) Field image of Unit 1 and 2; red line indicates non-travertine deposits. (C) Field image of Unit 2 representing horizontal layers. D) Field image of Unit 2 illustrating wavy lamination. (E, F) Field image of Unit 2 and 3 in NW and red line is boundary of exposure surface between them (yellow arrow is Unit 2 and red arrow is Unit 3) indicating system variation.

Fig. 5. Logs illustrating lithological variation along quarry walls (positions are indicated in quarry picture by L1 to L14). Colours indicate the individual lithotypes. The blue arrows show inferred flow direction of each unit. The grey “HP” areas indicate horizontal platforms that separate the individual excavation levels.

Fig. 6. Quarry walls illustrating different shrub morphologies. Red contour lines in pictures accentuate the morphology of peculiar features. (A, B, C) Alternation of dense and brightly white relatively thick deposits of dendriform shrub crusts (red arrows indicate individual crust layers). (D) Arbustiform shrubs. (E) Arborescent shrubs. (F) Field image of sub-rounded to rounded and cemented pustular shrubs. (G) Field image of radial shrub travertine. (I) Morphology classification of shrubs in function of proximal and distal position based on Claes et al. (20162017).

Fig. 7. Microphotographs illustrating different shrub lithotypes, their fabrics and associated pore types (in blue due to blue impregnation). Abbreviations used in the microphotographs: IDP = interdigitated growth framework porosity, ILP = interlaminar porosity, IP = intershrub growth framework porosity, MIP = microporosity, IAP = intrashrub growth framework porosity, C = sparite cement. (A) Thin-section scan showing different shrub types. (B) Crossed polarized image of dendritic shrub with needle-like thin and elongated branches possessing undulose extinction. (C) Compact and leaf-like branched shrub. (D) Micro-convex lamination of compact micrite and cement in dendritic shrub (red line). (E) Thick and elongated branches of dendritic shrubs. (F) Coexistence of pustular (red arrow) and dendritic shrub (blue arrow). (G) Pustular shrubs surrounded by calcite. (H) Radial shrub surrounded by calcite with internal lamination possibly of microbial origin. (I) Fluorescence microscopy of (H) showing green fluorescence at the edge of the radial shrubs.

Fig. 8. Field photograph of different lithotypes. (A) Dark coloured peloidal travertine occurring in between dendritic shrub crust. (B) Intercalation of dendritic shrub, pustular shrub and light coloured peloidal travertine with fenestral-like porosity. (C) Representative picture of vertical lithotype variation from dendritic shrub to non-travertine deposits, cryptalgal mudstone and eroded reed. (D) Combination of eroded reed and pustular shrub. (E) Intercalation between light coloured peloidal travertine and cryptalgal mudstone. (F) Field image of spongy microbial travertine (red line) with fenestral-like pores. (G and H) Field images with respectively in situ and eroded elongated reeds (now present as mouldic pores), occurring in a brown micritic matrix.

Fig. 9. Microphotographs of different non-shrub lithotypes, their fabrics and associated pore types. Abbreviations used in the microphotographs: FP = fenestral-like porosity, MP =

mouldic porosity, CVP = connected vuggy porosity, IPA = interparticle porosity, Pl = peloid, PS = pisoid. (A) Light colored micritic peloids with fenestral-like porosity (blue) and cement (white). (B) Dark colored peloidal travertine with intergranular porosity (blue) and cement (white). (C) Pisoid with micritic and peloidal nucleus and microsparitic cortex together with sub-rounded to rounded peloids. (D) Image of a reed mouldic pore (blue) surrounded by micritic dendrites. (E) Cryptalgal mudstone indicates cyanobacteria-like mudstone surrounded by cement. (F) Clumps of clotted micrite surrounded by cement. Pores filled with yellow resin. (G) Spongy porosity associated with connected vuggy porosity. (H) Image showing bundle of filaments. (I) Fluorescence microscopy image from (H) displaying bright fluorescence in the micritic wall parts of the filaments, while the cement infill and surrounding cement does not show fluorescence.

Fig. 10. non-travertine deposits and “in situ” reed. (A) View on non-travertine deposits at boundary between unit 1 and 2. (B) Close view of non-travertine deposits. The upper part consist of travertine fragments (red arrow). Notice the dissolution features above the non-travertine deposits. (C) “Dissolution cavity” with stalactite-like structures (green arrow) and banded cement (red arrow). (D) Dissolution cavity partially filled by rafts and silty lime-mud (red arrow) that display a geopetal arrangement. (E) Dissolution cavity with banded cement (red arrow). (F) Solution enlarged reed structure (red arrow).

Fig. 11. Diagenetic features associated with sub-horizontal travertine. (A) Isopachous banded crystals with micrite interlayers (see red arrows). (B and C) Bladed calcite cement surrounding clotted micrite. (D) Blocky calcite cement (red arrow) occurring between clotted micrite. (E) Sub-heudral to equant calcite cement (red arrow) filling the pore space between peloids. (F and G) Polarized and fluorescent light image showing different generations of cement and its partial dissolution creating some microporosity. (H) Meniscus calcite at or near peloid and pisoid grain. (I) Geopetal fabric in gastropod with internal fillings of both

cement and micrite. (J) Neomorphism of clotted micrite (red arrow). (K) Bioturbation (red arrow) and green algae (green arrow). (L) Micritic coating (red arrow) interpreted as calcrete microstructure related to pedogenesis.

Fig. 12. Diagenetic features associated with sub-horizontal travertines. (A) Mouldic porosity in gastropods. (B, C) Transmitted light and cathodoluminescence image of microsparitic fabric showing some luminescence in clotted micrite. (D) SEM image of organic structure in spongy lithotype. (E) Acicular crystals (red arrow), possibly testifying of the former presence of aragonite. (F) SEM image of micropores (red arrow) in spongy travertine. (G) Crossed polarized light image of undulose extinction in re-crystallised fibrous cement. (H and I) Transmitted and fluorescent light image showing filamentous structures with microporosity. (J) Cemented fracture (red arrow) in micrite with calcite cemented vugs.

Fig. 13. Cross plot of stable carbon versus oxygen isotopes of different sparite and micrite (respectively red and green squares) from the study area, compared with encircled fields of travertine that formed in similar hydrogeological and hydrodynamic contexts according to Teboul et al. (2016).

Fig. 14. Cross plot of stable oxygen versus carbon isotopes of the different units from the study area.

Fig. 15. Vertical evolution and box plots of the carbon isotope composition within the 3 units. In Unit 1 and 2 almost all couples show depleted cement with respect to micrite signatures.

Fig. 16. Vertical evolution and box plots of oxygen isotope signature within the 3 units. In Unit 1 micrite generally possesses lower oxygen isotope signatures than cement, while it is the reverse within Unit 2.

Fig. 17. Cross plot of C/N ratio versus organic $\delta^{13}C$ from the Sub-horizontal facies in the Çakmak quarry (red points), with fields of interpreted origins according to Meyers (1994).

Fig. 18. Logarithmic cross plot of strontium versus barium from the sub-horizontal facies in Çakmak quarry. Blue points represent the dataset acquired in this study. They are plotted in the "fields of origin" reported by Teboul et al. (2016).

Fig. 19 Paleoenvironmental model for the extensive depressional setting in Çakmak quarry. Vertical variation of the three described units as a function of direction in water flow and orientation of the lithological layer. The first unit reflects a shallow depression of both lacustrine (sub-aqueous in blue) and palustrine (sub-aerial in grey) origin. Unit 2 starts with shrub micro-terraces with $<5^0$ dip varying laterally into marsh environment. Unit 3 starts with smooth slope with some small-sized pool rims constituted of reeds that laterally evolves in a marsh setting.

Figures

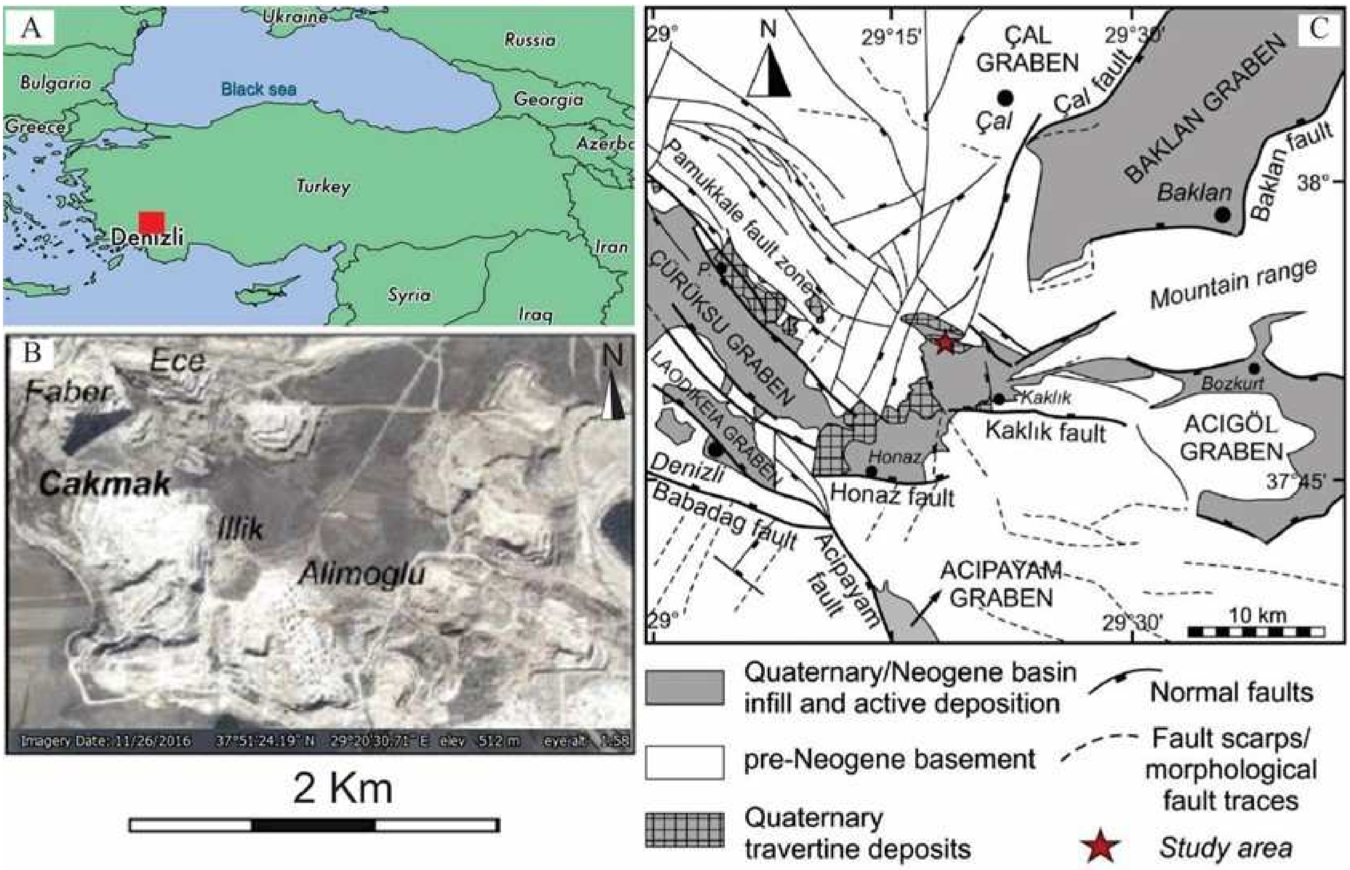
A
Ukraine
Russia
Bulgaria
Black sea
Georgia
Greece
Azerba
Turkey
Denizli
Iran
Syria
Iraq
B
Ece
Faber
Cakmak
Illik
Alimoglu
N
Imagery Date: 11/26/2016 37°51'24.19" N 29°20'30.71" E elev 512 m
2 Km
C
29°
N
29°15'
ÇAL GRABEN
29°30'
Çal
Çal fault
BAKLAN GRABEN
Baklan fault
Baklan
38°
Pamukkale fault zone
ÇÜRÜKSU GRABEN
Mountain range
LAODIKEIA GRABEN
Kaklık
Bozkurt
Kaklık fault
ACIGÖL GRABEN
Denizli
Honaz
Honaz fault
37°45'
Babadag fault
Acipayam fault
ACIPAYAM GRABEN
29°
29°30'
10 km
Quaternary/Neogene basin infill and active deposition
Normal faults
pre-Neogene basement
Fault scarps/ morphological fault traces
Quaternary travertine deposits
Study area

Figure 1

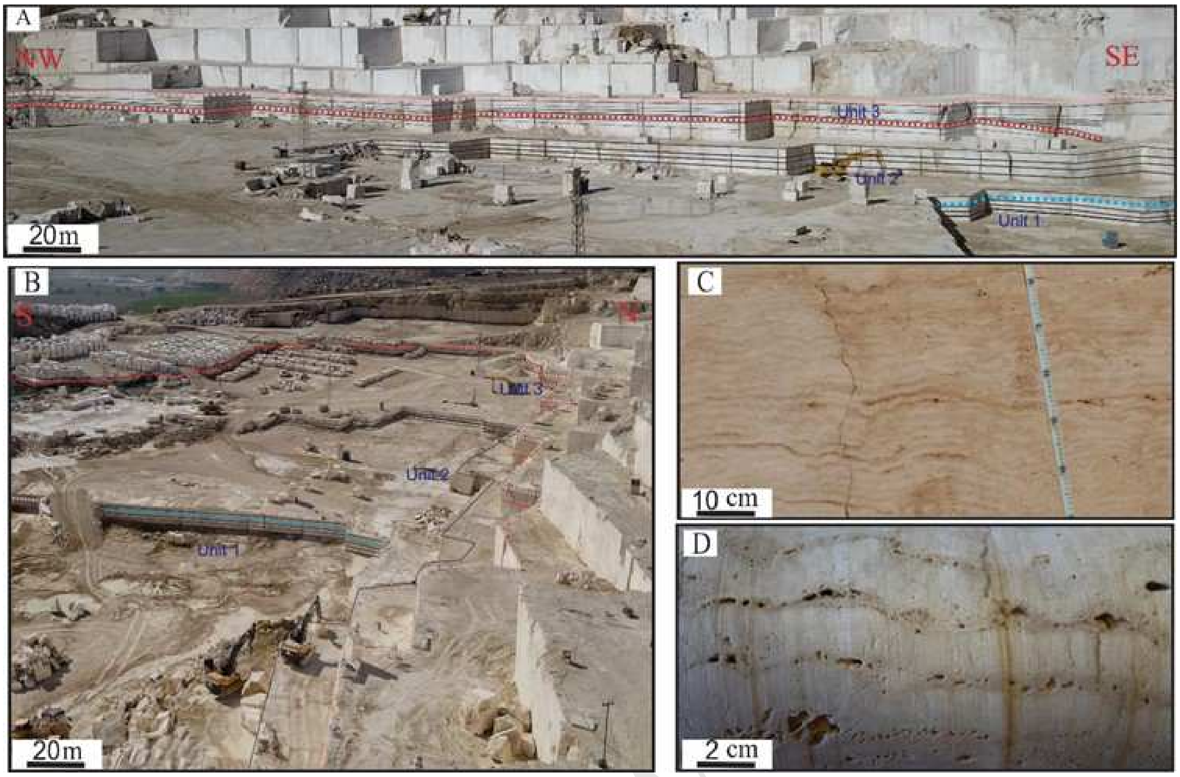
A
NW
SE
Unit 3
Unit 2
Unit 1
20m
B
Unit 3
Unit 2
Unit 1
20m
C
10 cm
D
2 cm

Figure 2

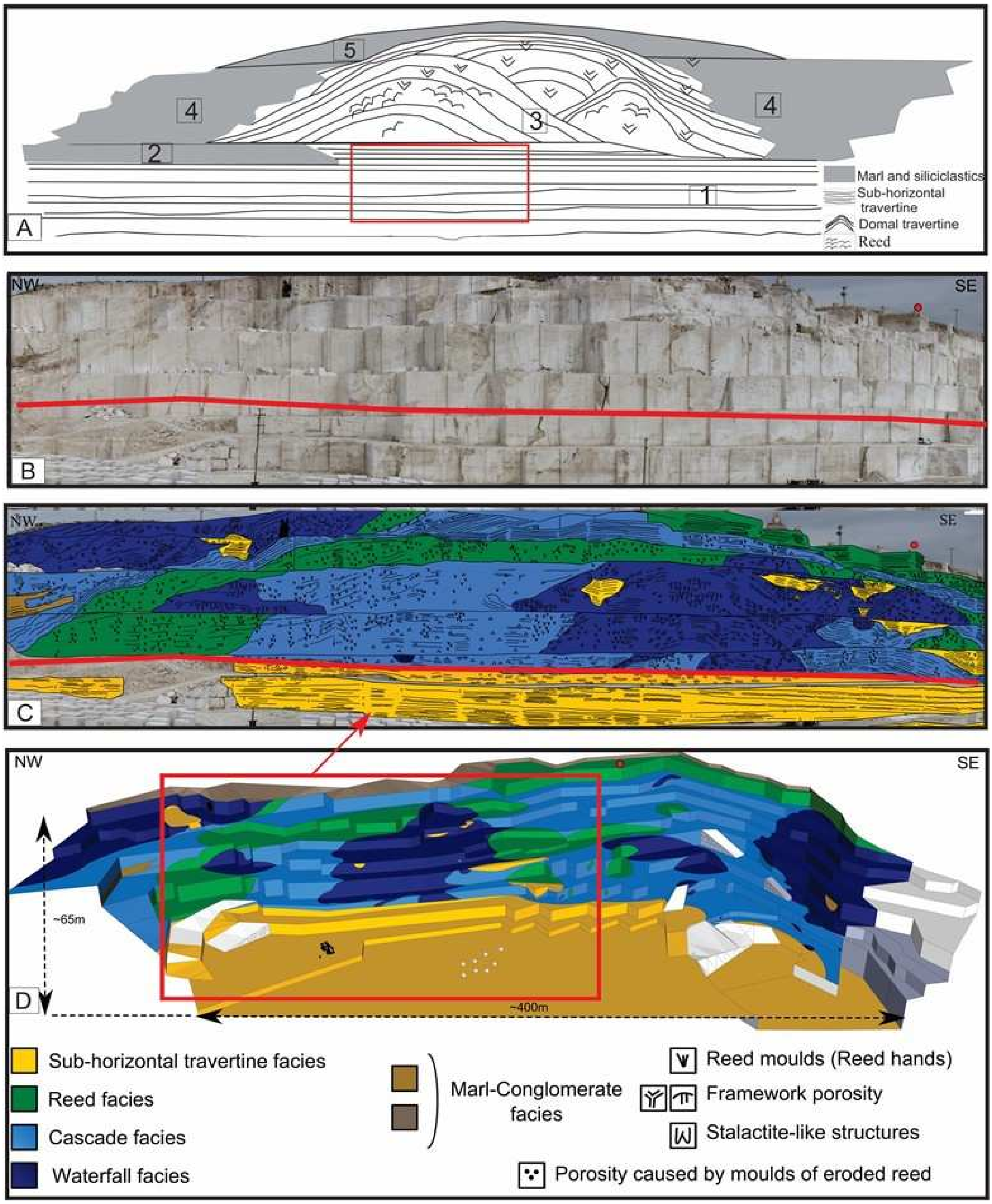
5
4
3
4
2
1
A
Marl and siliciclastics
Sub-horizontal travertine
Domal travertine
Reed
NW
SE
B
NW
SE
C
NW
SE
~65m
D
~400m
Sub-horizontal travertine facies
Reed facies
Cascade facies
Waterfall facies
Marl-Conglomerate facies
Reed moulds (Reed hands)
Framework porosity
Stalactite-like structures
Porosity caused by moulds of eroded reed

Figure 3

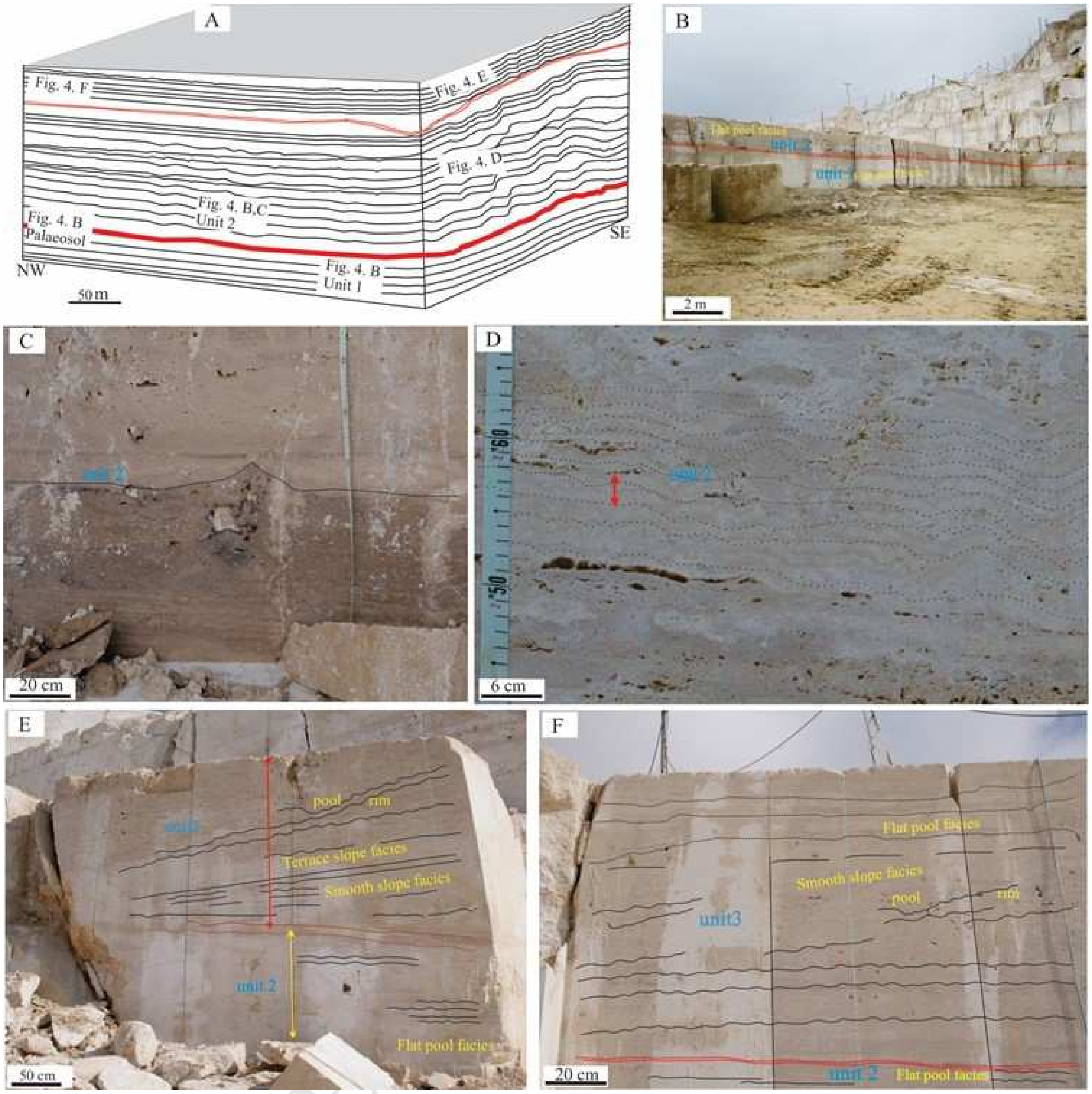
A
Fig. 4. F
Fig. 4. E
Fig. 4. D
Fig. 4. B,C
Unit 2
Fig. 4. B
Palaeosol
NW
SE
Fig. 4. B
Unit 1
50 m
B
unit 2
unit 1
2 m
C
unit 2
20 cm
D
unit 2
6 cm
E
pool
rim
Terrace slope facies
Smooth slope facies
unit 2
Flat pool facies
50 cm
F
Flat pool facies
Smooth slope facies
pool
rim
unit3
20 cm
unit 2
Flat pool facies

Figure 4

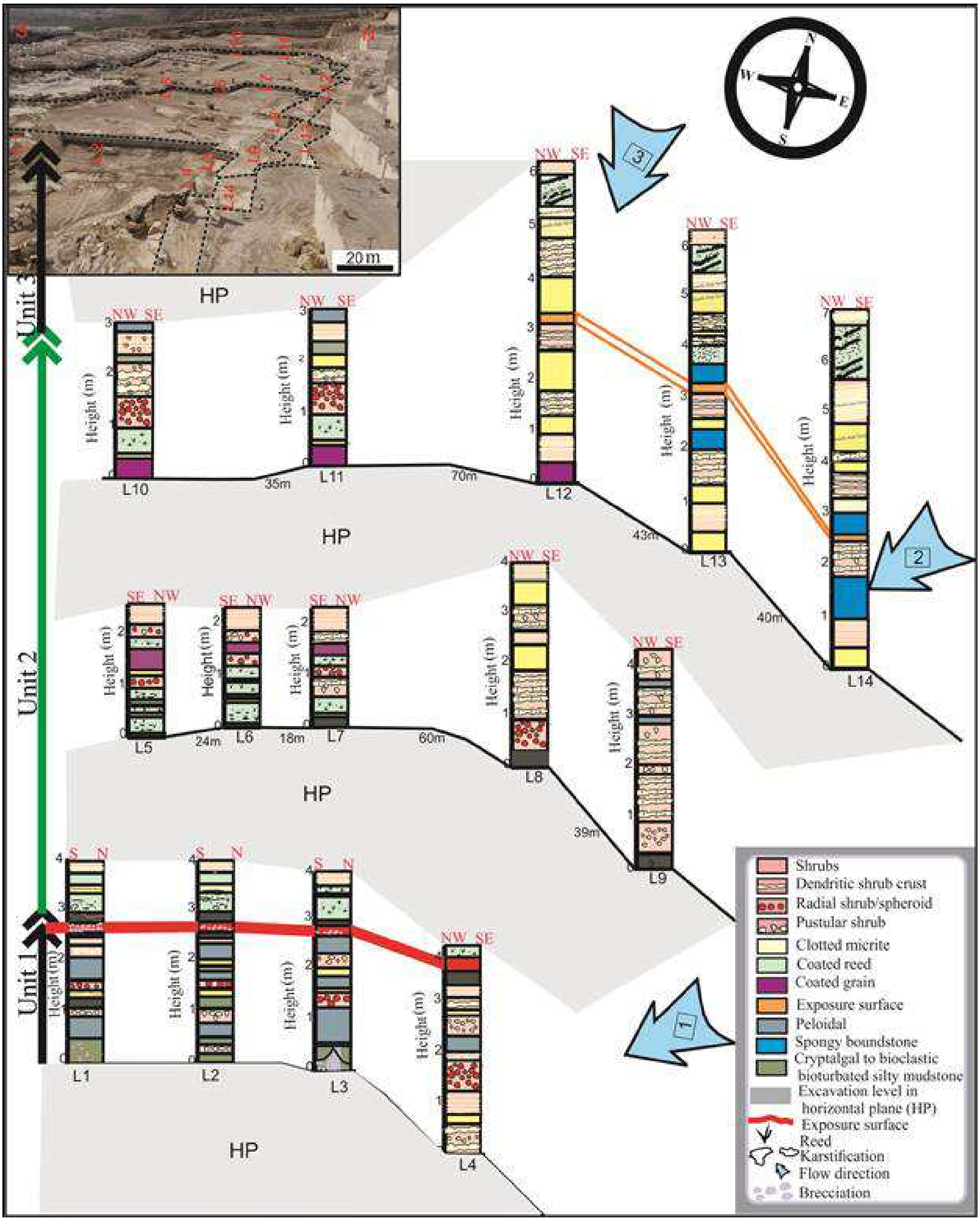

20 m
HP
Unit 1
Unit 2
Unit 3
Height (m)
NW SE
SE NW
S N
L1
L2
L3
L4
L5
L6
L7
L8
L9
L10
L11
L12
L13
L14
35m
70m
43m
40m
24m
18m
60m
39m
1
2
3
N
W
E
S
Shrubs
Dendritic shrub crust
Radial shrub/spheroid
Pustular shrub
Clotted micrite
Coated reed
Coated grain
Exposure surface
Peloidal
Spongy boundstone
Cryptalgal to bioclastic bioturbated silty mudstone
Excavation level in horizontal plane (HP)
Exposure surface
Reed
Karstification
Flow direction
Brecciation

Figure 5

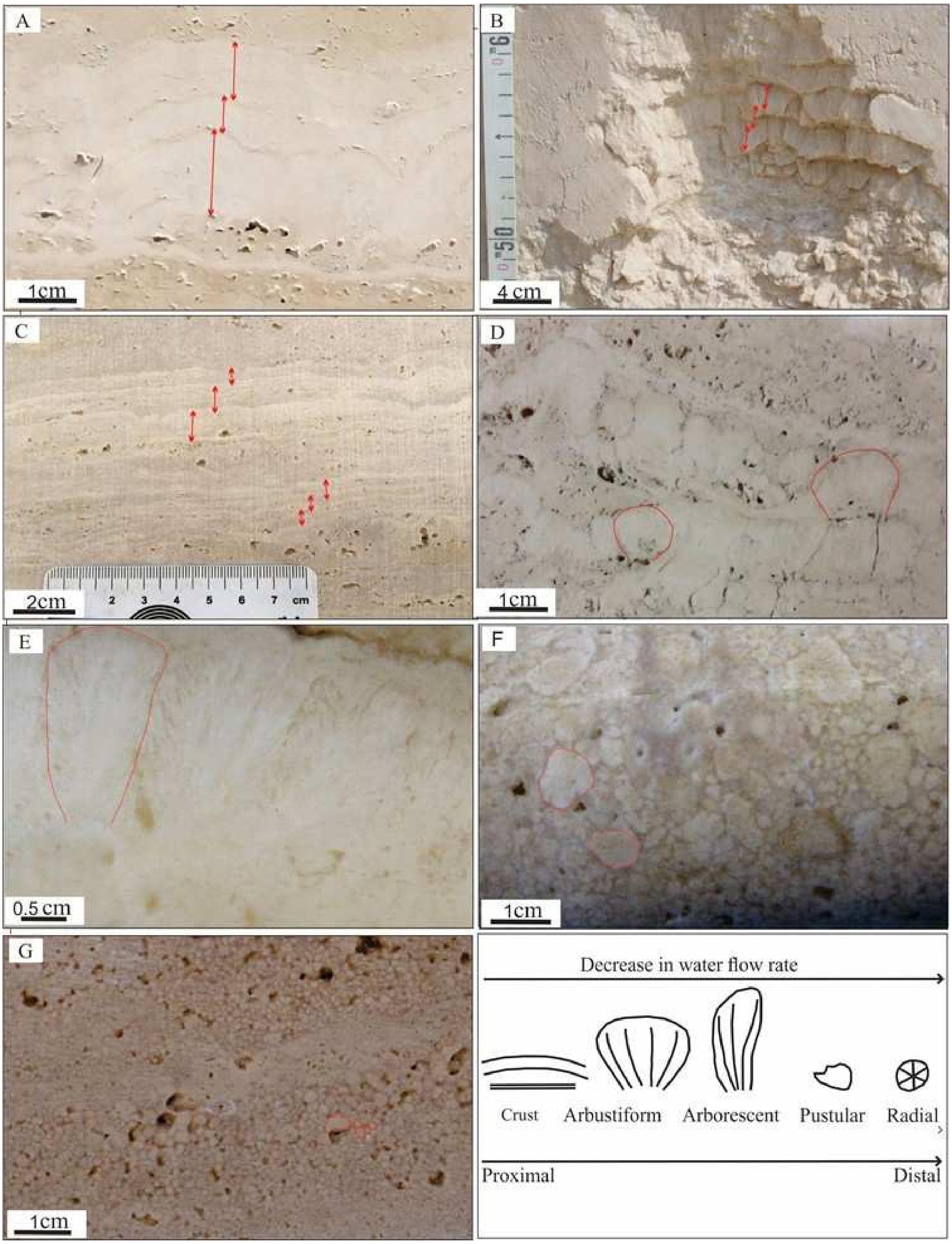
A
1cm
B
4 cm
C
2cm
D
1cm
E
0.5 cm
F
1cm
G
1cm
Decrease in water flow rate
Crust
Arbustiform
Arborescent
Pustular
Radial
Proximal
Distal

Figure 6

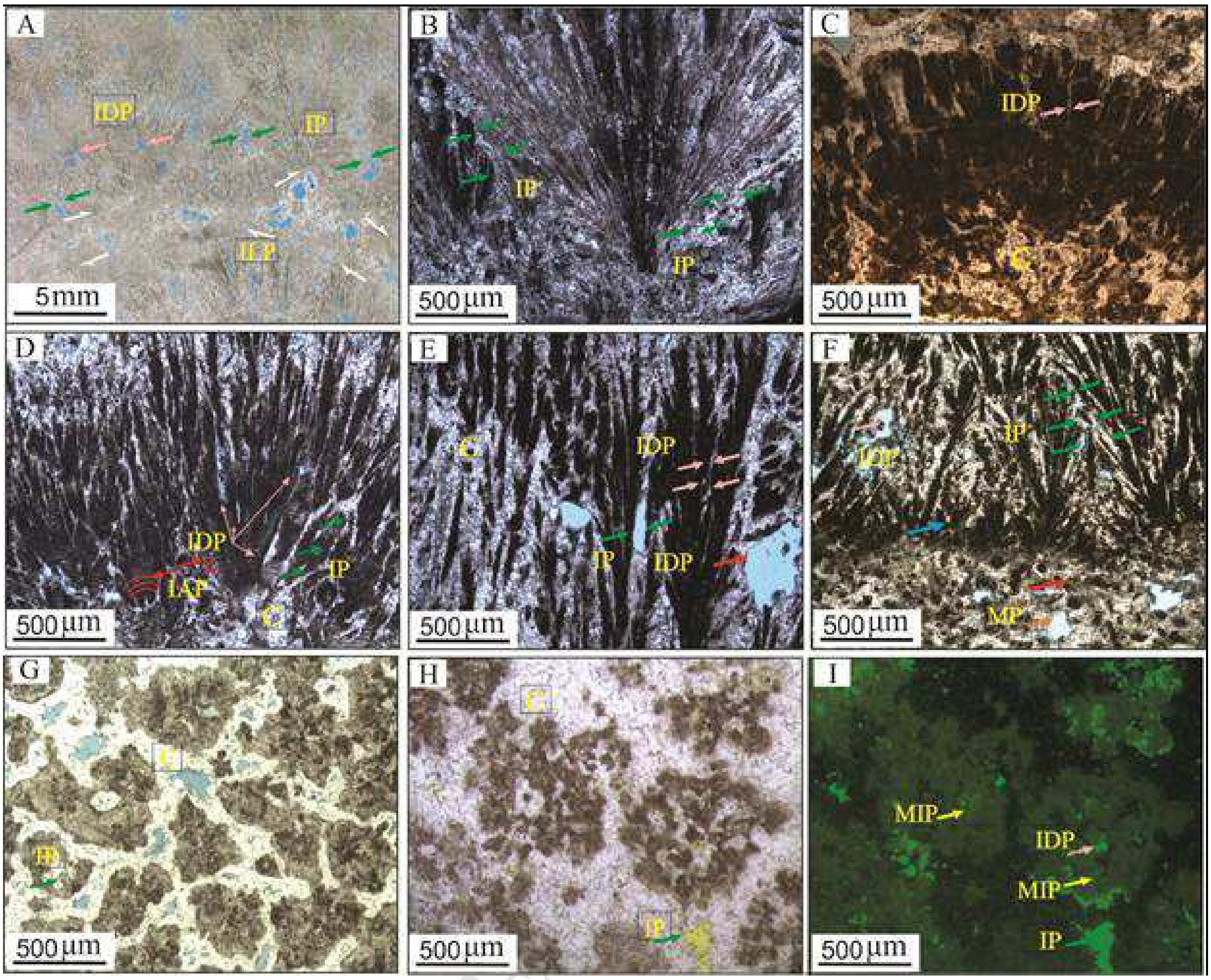
A
IDP
IP
ILP
5mm
B
IP
IP
500 μm
C
IDP
C
500 μm
D
IDP
IAP
IP
C
500 μm
E
C
IDP
IP
IDP
500 μm
F
IDP
IP
MP
500 μm
G
C
IP
500 μm
H
C
IP
500 μm
I
MIP
IDP
MIP
IP
500 μm

Figure 7

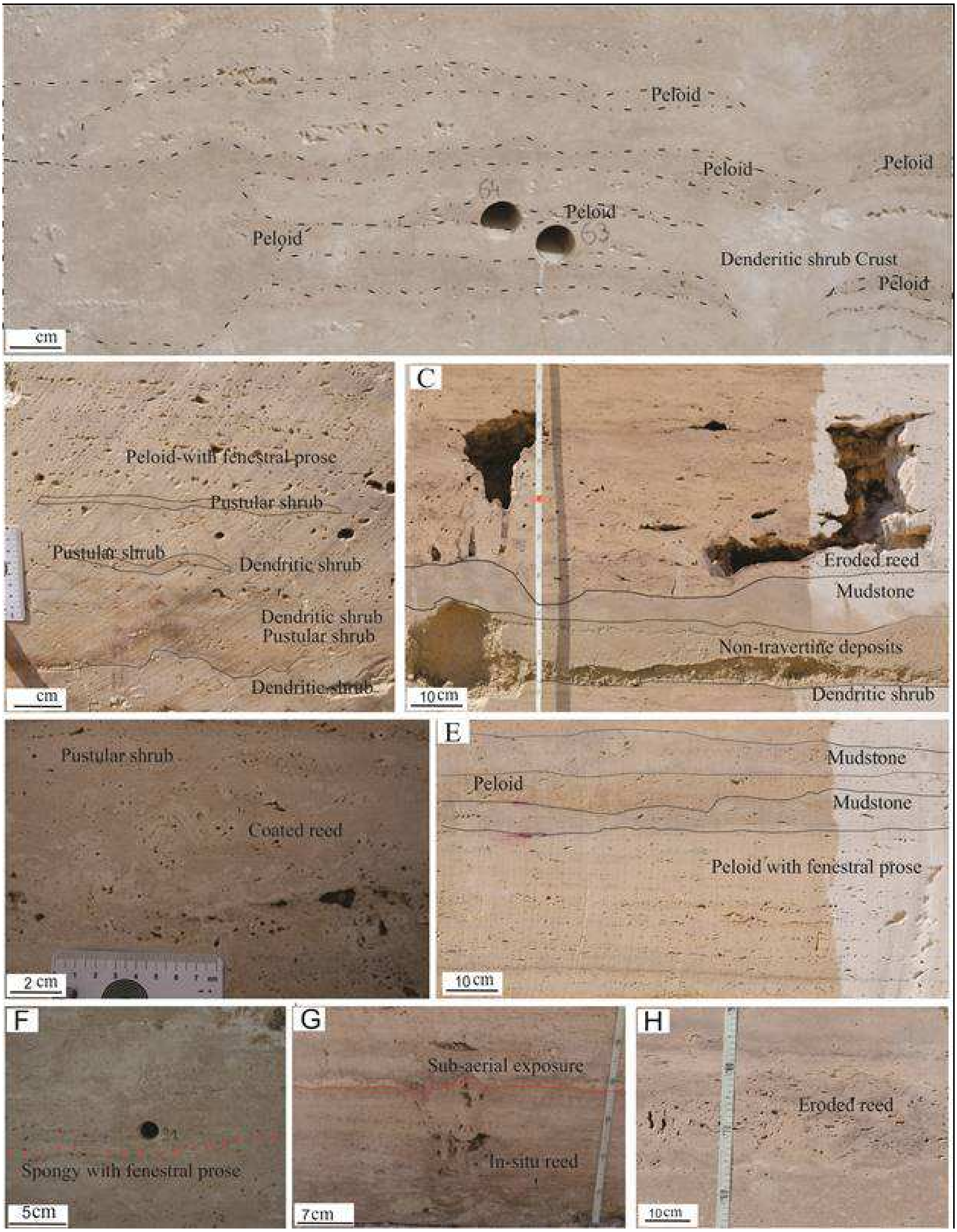
Peloid
Peloid
Peloid
Peloid
Peloid
Denderitic shrub Crust
Peloid
cm
Peloid-with fenestral prose
Pustular shrub
Pustular shrub
Dendritic shrub
Dendritic shrub
Pustular shrub
Dendritic shrub
cm
C
Eroded reed
Mudstone
Non-travertine deposits
Dendritic shrub
10cm
Pustular shrub
Coated reed
2 cm
E
Mudstone
Peloid
Mudstone
Peloid with fenestral prose
10cm
F
Spongy with fenestral prose
5cm
G
Sub-aerial exposure
In-situ reed
7cm
H
Eroded reed
10cm

Figure 8

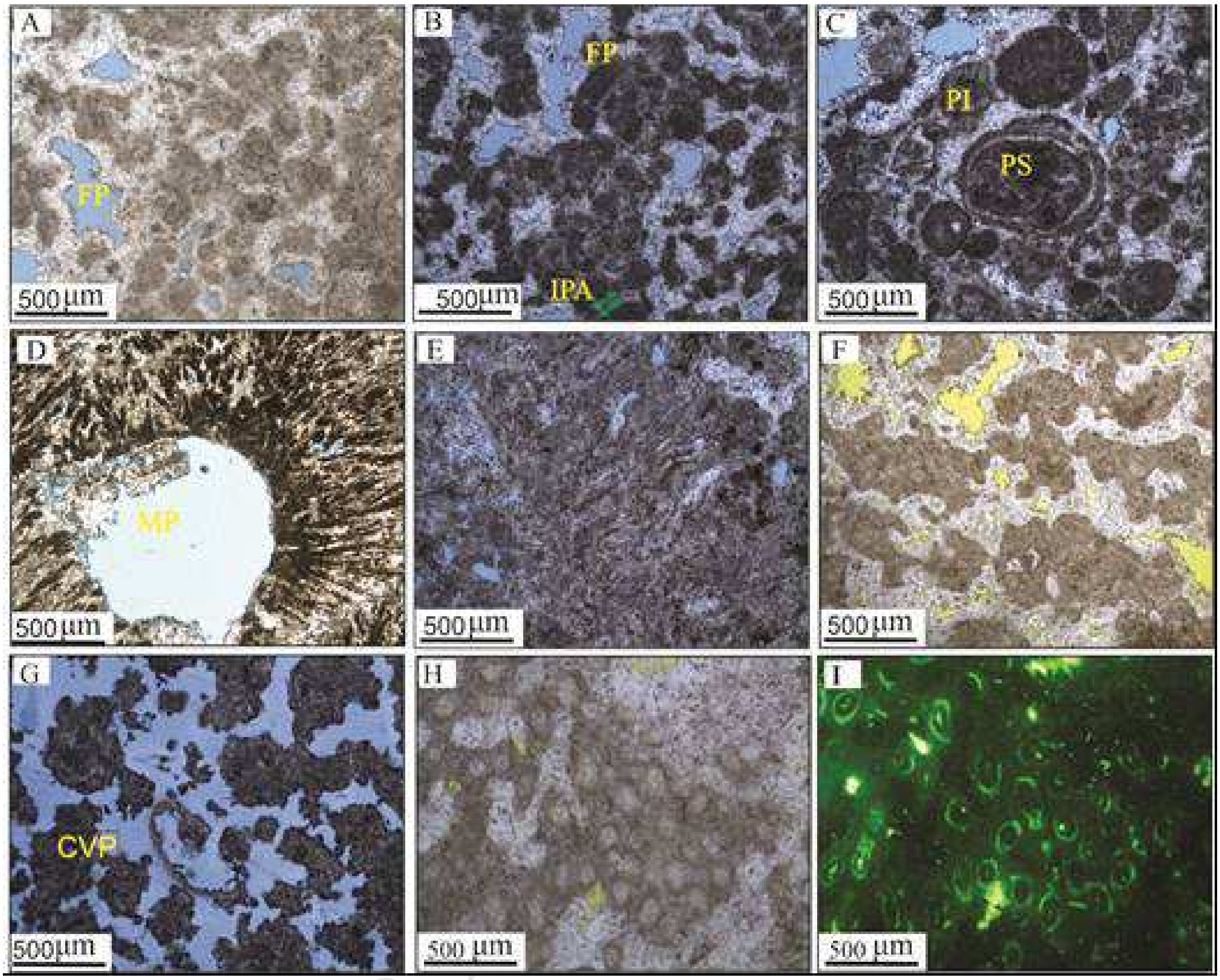
A
FP
500μm
B
FP
500μm
IPA
C
PI
PS
500μm
D
MP
500μm
E
500μm
F
500μm
G
CVP
500μm
H
500 μm
I
500 μm

Figure 9

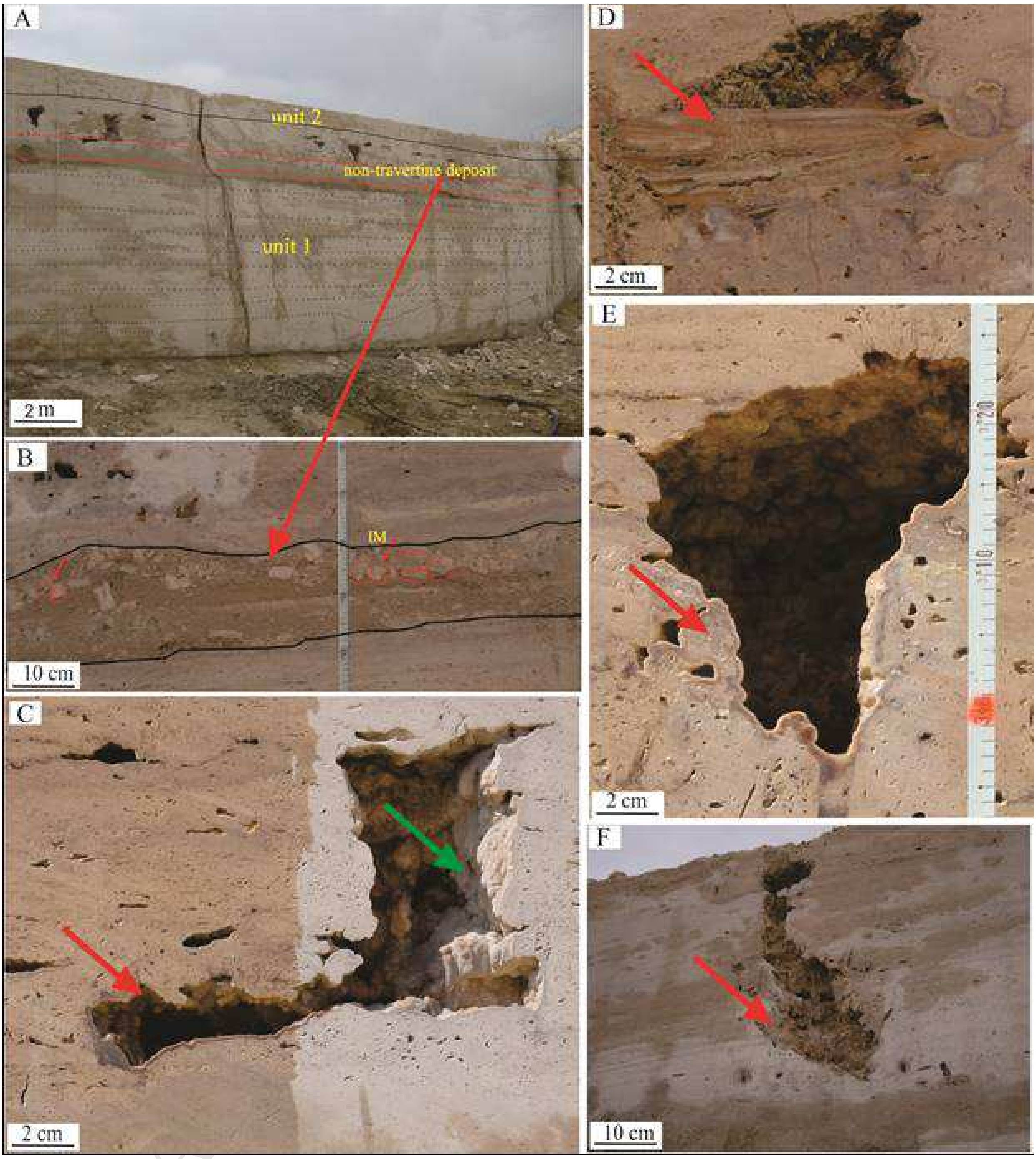
A
unit 2
non-travertine deposit
unit 1
2 m
B
IM
10 cm
C
2 cm
D
2 cm
E
2 cm
F
10 cm

Figure 10

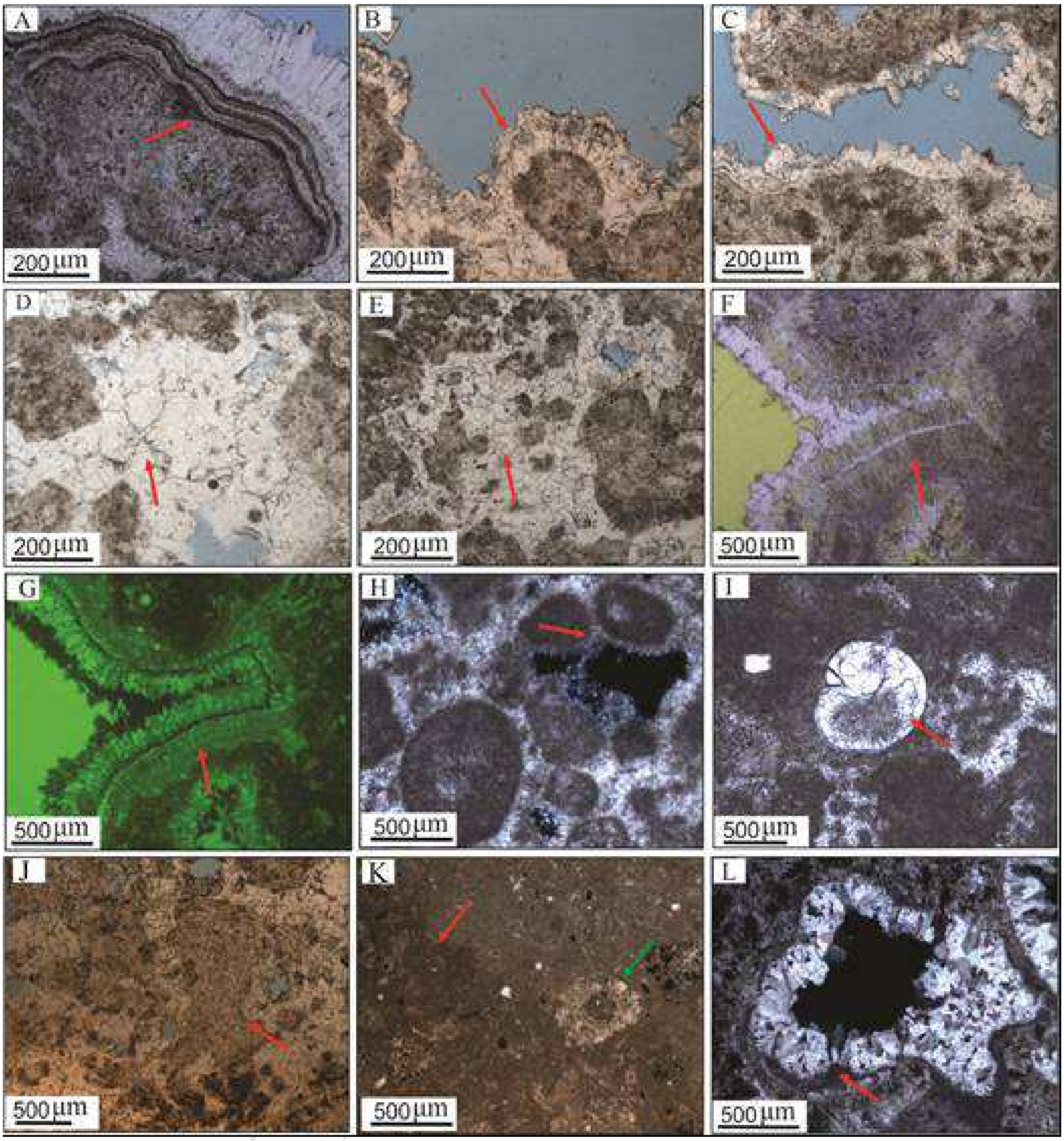
A
200 μm
B
200 μm
C
200 μm
D
200 μm
E
200 μm
F
500 μm
G
500 μm
H
500 μm
I
500 μm
J
500 μm
K
500 μm
L
500 μm

Figure 11

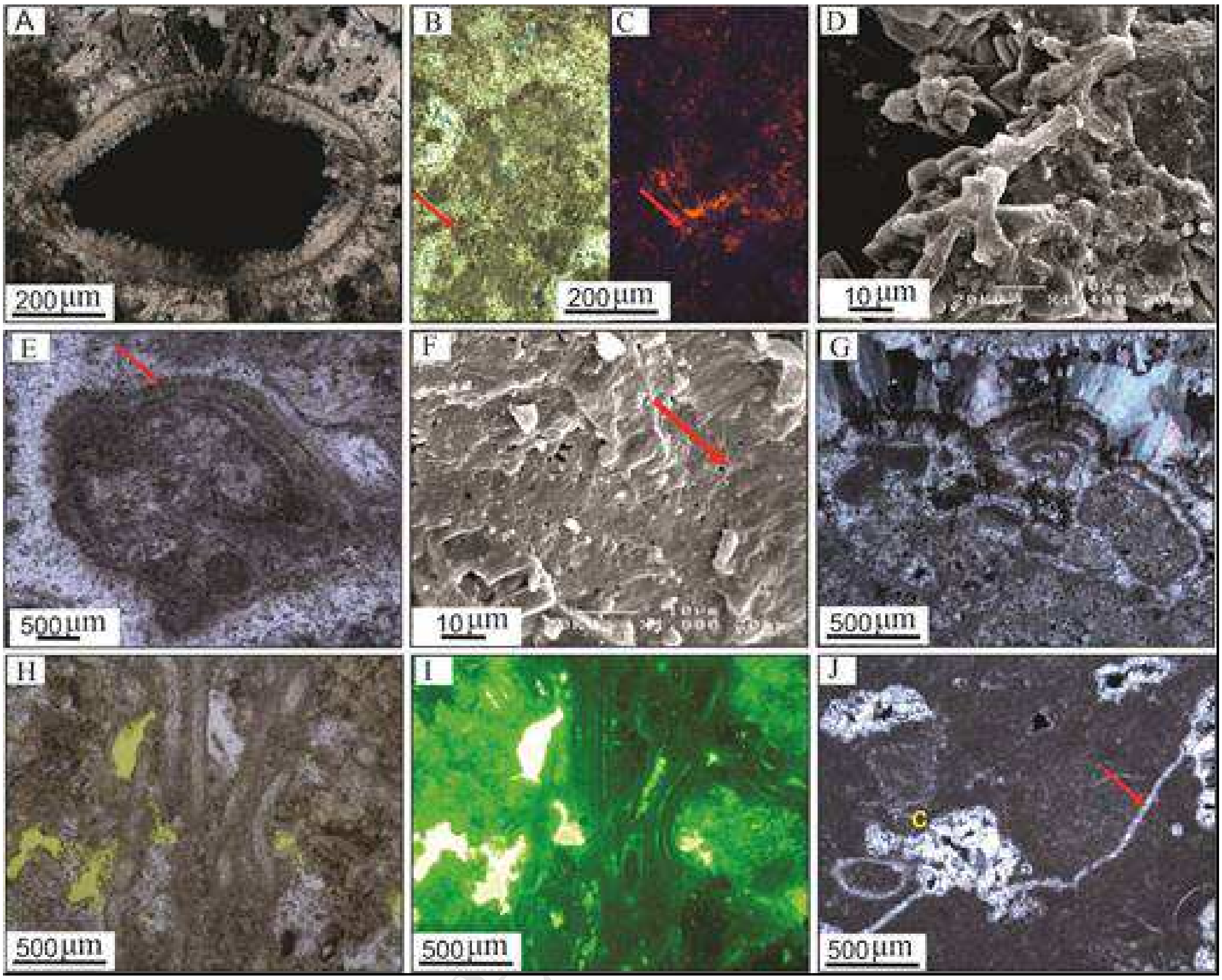
A
200 µm
B
C
200 µm
D
10 µm
E
500 µm
F
10 µm
G
500 µm
H
500 µm
I
500 µm
J
C
500 µm

Figure 12

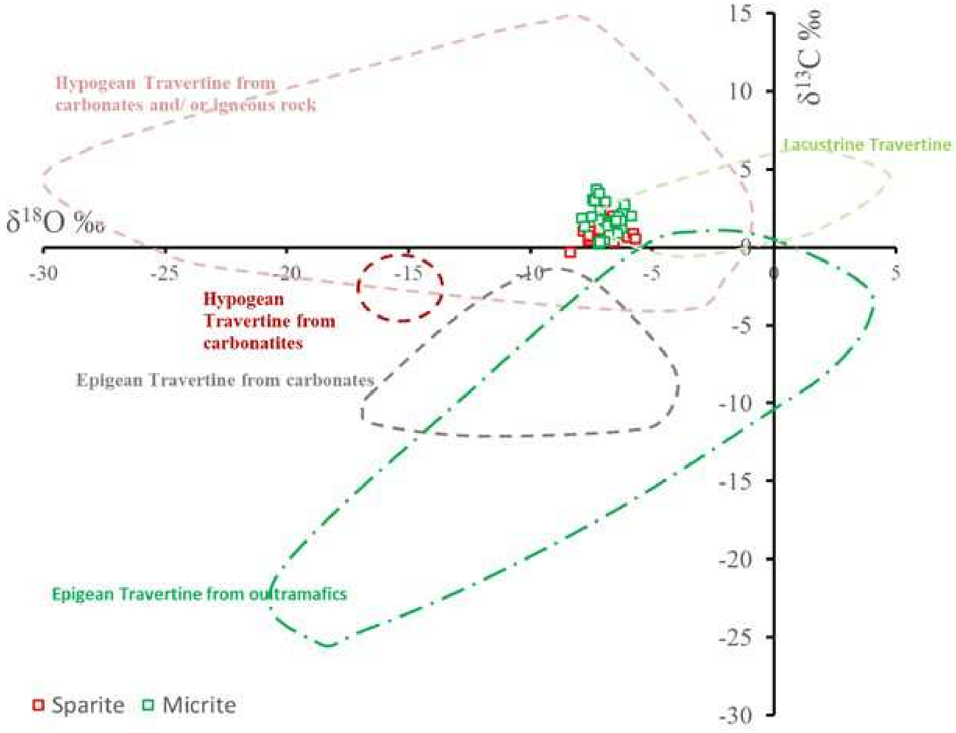

Hypogean Travertine from carbonates and/ or igneous rock
Lacustrine Travertine
δ18O ‰
δ13C ‰
Hypogean Travertine from carbonatites
Epigean Travertine from carbonates
Epigean Travertine from oultramafics
Sparite
Micrite

Figure 13

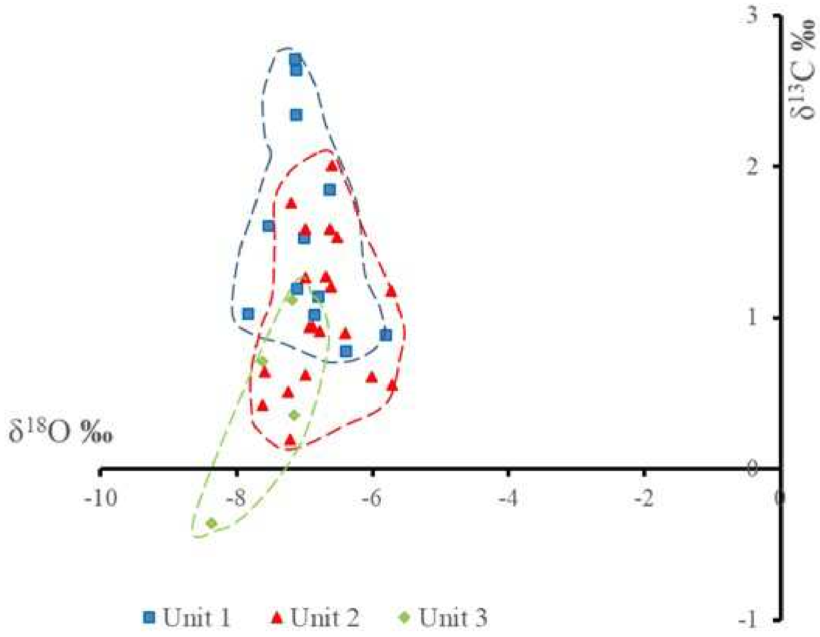

δ18O ‰
δ13C ‰
Unit 1
Unit 2
Unit 3

Figure 14

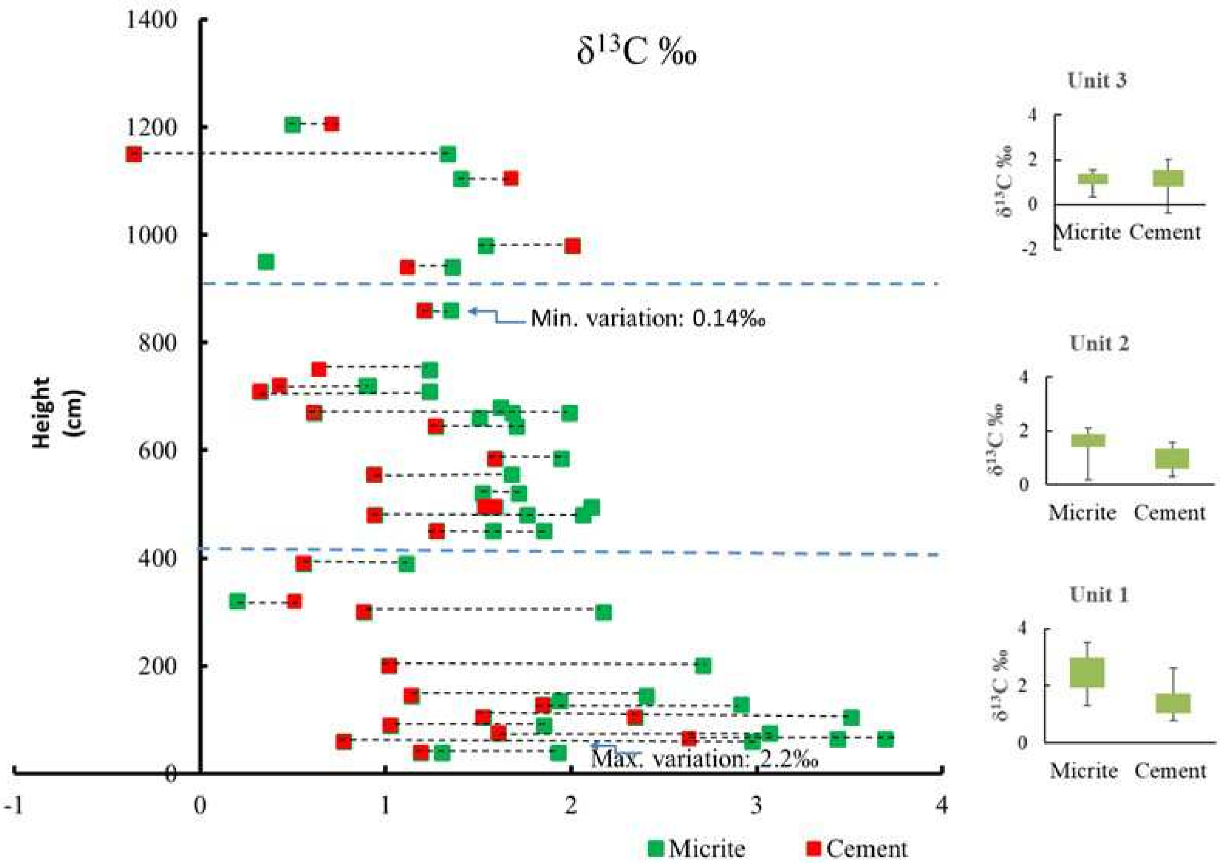

Figure 15

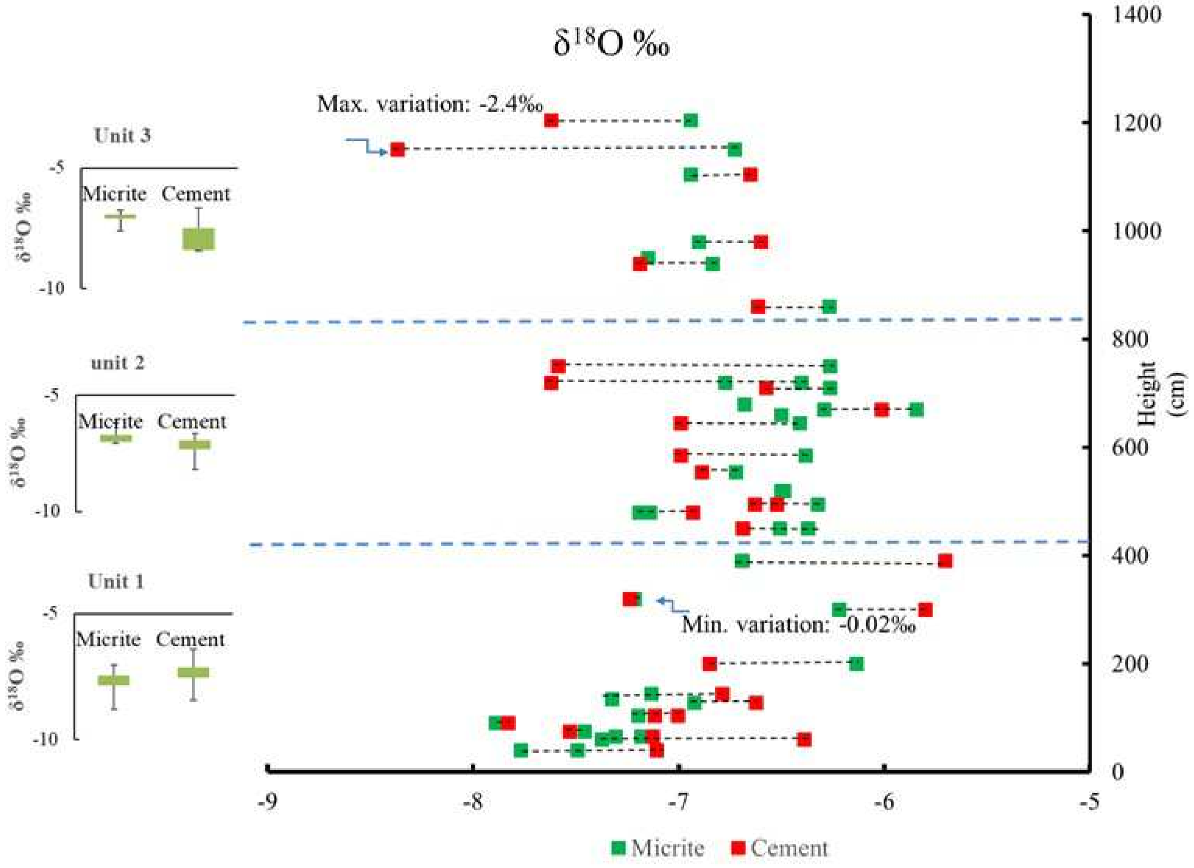
δ18O ‰
Max. variation: -2.4‰
Min. variation: -0.02‰
Unit 3
unit 2
Unit 1
Micrite
Cement
δ18O ‰
-5
-10
1400
1200
1000
800
600
400
200
0
Height (cm)
-9
-8
-7
-6
-5
Micrite
Cement

Figure 16

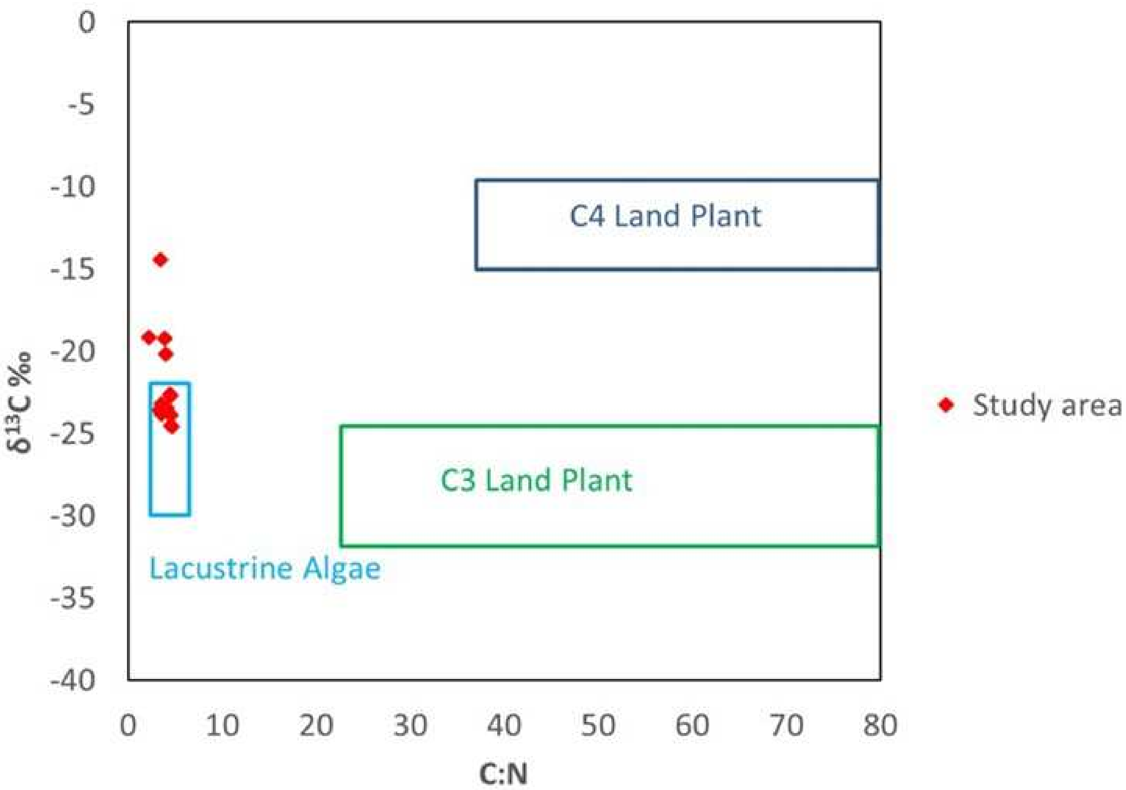
0
-5
-10
-15
-20
-25
-30
-35
-40
δ¹³C ‰
0
10
20
30
40
50
60
70
80
C:N
C4 Land Plant
C3 Land Plant
Lacustrine Algae
Study area

Figure 17

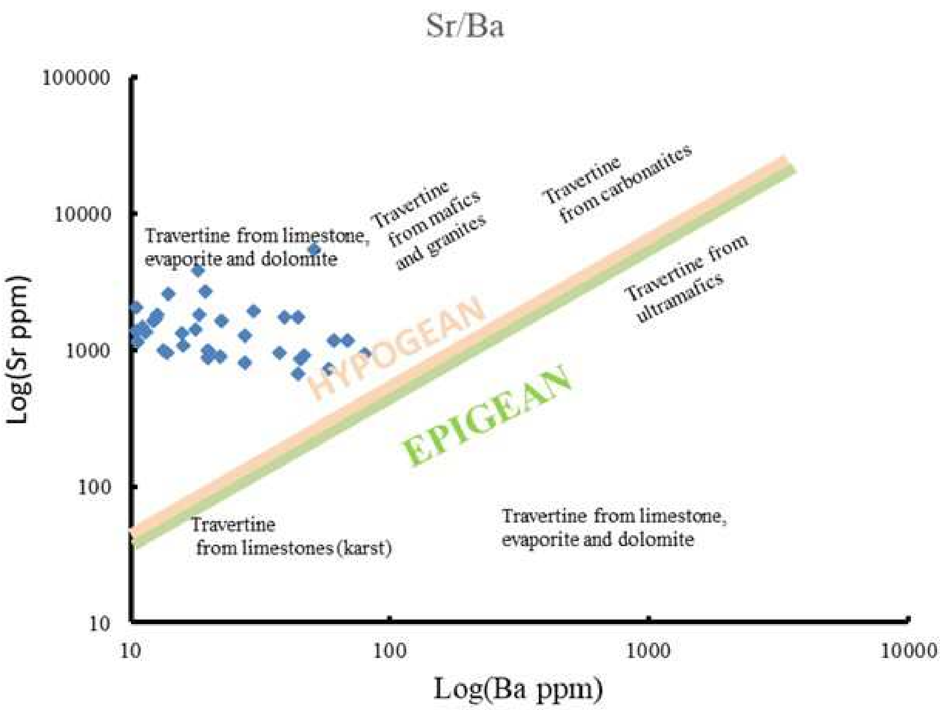
Sr/Ba
100000
10000
1000
100
10
Log(Sr ppm)
10
100
1000
10000
Log(Ba ppm)
Travertine from limestone, evaporite and dolomite
Travertine from mafics and granites
Travertine from carbonatites
Travertine from ultramafics
HYPOGEAN
EPIGEAN
Travertine from limestones (karst)
Travertine from limestone, evaporite and dolomite

Figure 18

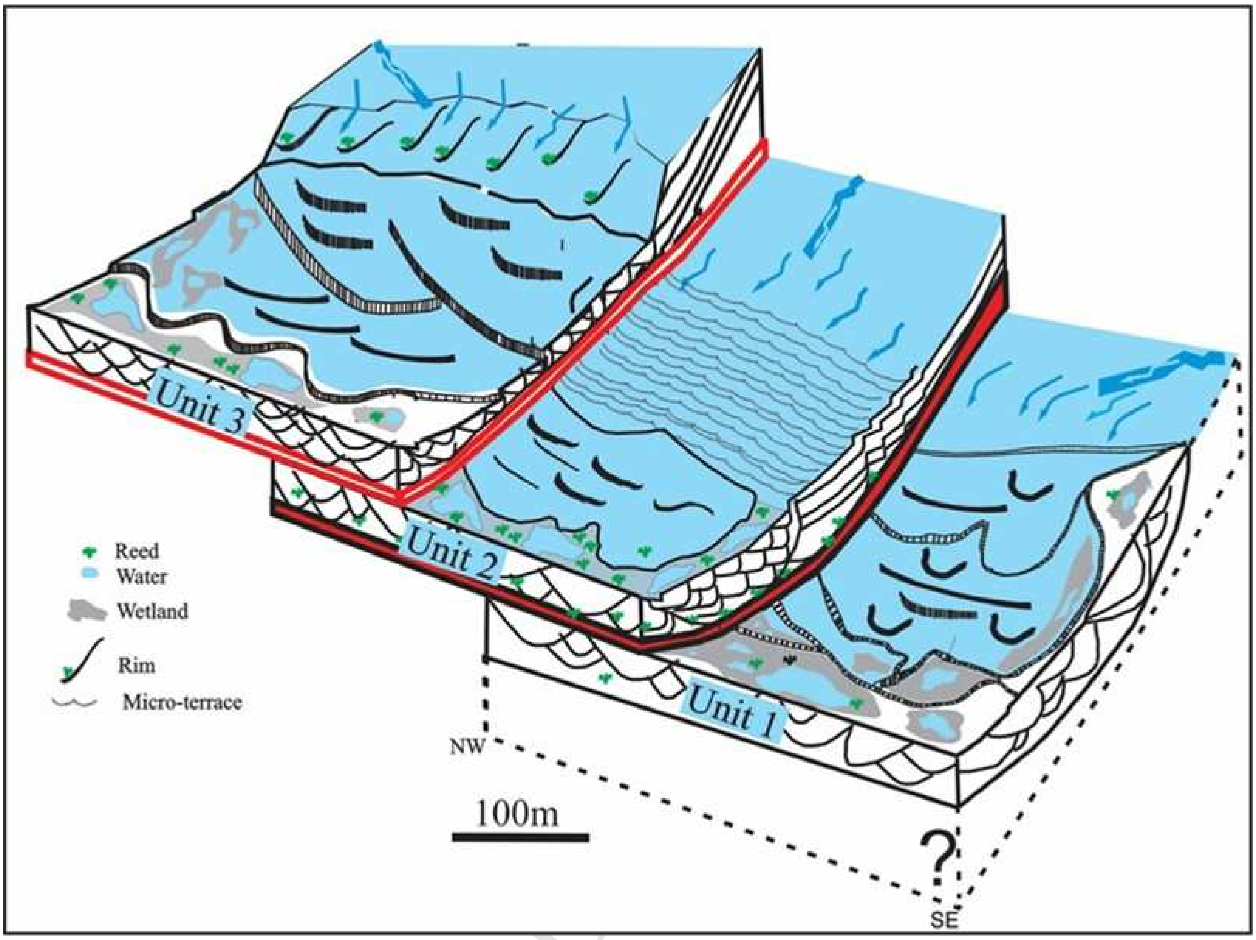

Unit 3
Unit 2
Unit 1
Reed
Water
Wetland
Rim
Micro-terrace
NW
SE
100m
?

Figure 19